IEEE Access
Multidisciplinary | Rapid Review | Open Access Journal

Received April 1, 2020, accepted April 17, 2020, date of publication April 30, 2020, date of current version May 15, 2020.

Digital Object Identifier 10.1109/ACCESS.2020.2991417

Heuristic Chaotic Hurricane-Aided Efficient Power Assignment for Elastic Optical Network

LAYHON R. RODRIGUES DOS SANTOS[1] AND TAUFIK ABRÃO[2], (Senior Member, IEEE)
[1]Department of Electrical Engineering, Technological Federal University, Cornélio Procópio 86300-000, Brazil
[2]Department of Electrical Engineering, Londrina State University, Londrina 86057-970, Brazil

Corresponding author: Layhon R. Rodrigues dos Santos (lay.lyns@hotmail.com)

This work was supported in part by the National Council for Scientific and Technological Development (CNPq) of Brazil under Grant 304066/2015-0, in part by the Coordenação de Aperfeiçoamento de Pessoal de Nível Superior-Brazil (CAPES)-Finance Code 001, in part by the Londrina State University (UEL), in part by the Paraná State Government, and in part by the CAPES and Federal University of Technology-Parana State (UTFPR).

ABSTRACT In this paper, we propose a dynamical power allocation (PA) procedure for elastic optical networks (EONs) based on the evolutionary hurricane search optimization (HSO) algorithm with a chaotic logistic map diversification strategy with the purpose of improving the capability to escape from local optima, namely PA-CHSO. The aiming is the dynamical control of the transmitted optical powers according to the variations of each link state due to traffic fluctuations, channel impairments, as well as other channel-power coupling effects. Such realistic EON scenarios are affected mainly by the channel estimation inaccuracy, channel ageing and power fluctuations. The link state is based on the channel estimation and quality of transmission (QoT) parameters obtained from the optical performance monitors (OPMs). Numerical results have demonstrated the effectiveness of the PA-CHSO to dynamically mitigate the power penalty under real measurement conditions with uncertainties and noise, as well as when perturbations in the optical transmit powers are considered.

INDEX TERMS Adaptive power control algorithm, optical networks, hurricane algorithm, chaotic map, elastic optical networks.

I. INTRODUCTION

The growth of the traffic demand with heterogeneous characteristics associated to the increment of the SNR rate requirements has pressing the development of dynamical optical networks. Currently, the technological maturity of devices, equipment and protocols provides the use of dynamical flexible grid-rate elastic optical network (EON). In the EONs, the lightpaths with adjustable bandwidth, modulation level and spectrum assignment can be established according to actual traffic demands and quality of service (QoS) requirements [1], [2]. In addition, the quality of transmission (QoT) of each lightpath is evaluated previously to resources allocation purpose, as well as to obtain reliable optical connectivity [2], [3]. The best knowledge of the QoT is needed in the design and operation phases, owing to the margin has to be added in the network when the QoT is not well established [4]. The QoT prediction can utilizes different methodologies based on sophisticated analytical models, approximated formulas and optical performance monitors (OPMs) [4], [5]. The QoT estimation with OPMs distributed in the route or in the coherent receiver can be appropriated in term of precision and computational complexity (CC) when integrated in to the active control plane to provide the link conditions in real time [1], [3]. However, it is important to consider the limited accuracy of the OPMs that increase the measurements uncertainty considering the channel impairments (including linear and nonlinear effects), receiver architecture and noise, which decrease the performance of the channel state estimation [5], [6]. In addition, the power dynamics related to the channel-power coupling effects, which are influenced by the network topology, traffic variation, physics of optical amplifiers and the dynamic addition and removal of lightpaths can cause optical channel power instability and result in QoT degradation [1]. Moreover, the interactions between lighpaths in some routes of the network can generate fluctuations to form closed loops and create disruptions.

The power, routing, modulation level and spectrum assignment (PRMSA) problem is usually determinate in the

The associate editor coordinating the review of this manuscript and approving it for publication was Rentao Gu.

planning stage of the network and margins are included considering the QoT inaccuracies, equipment ageing, inter-channel interference, as well as the uncertainties of the optical power dynamics [7], [8]. However, there are some investigations to the development of resource allocation algorithms based on OPMs with reduced margins, which have considered ageing and inter-channel interference to configurable transponders with launch powers [5], regenerator placement [4] and the optimization of the physical topology for power minimization [9]. These algorithms can be based on derivative-free optimization (DFO), constrained direct-search algorithms [5], and mixed integer linear programming (MILP) [9]. Furthermore, in [6] an adaptive proportional-integral-derivative (PID) with gains auto-tuning based on particle swarm optimization (PSO) to dynamically control the transmitted power according to the OPMs measurements for mixed line rate (MLR) was proposed. Previous investigations for the legacy single rate network for power control adjustment to the optical-signal-to-noise-ratio (OSNR) optimization considering the physical impairments were conducted based on a game-theory-based [10] and (PID) back propagation (BP) neural networks [11]. Moreover, the power allocation (PA) optimization aiming at obtaining energy-efficient optical CDMA systems using different programming methods is carried out in [12]. Such optimization methods, including augmented Lagrangian method (ALM), sequential quadratic programming method (SQP), majoration-minimization (MaMi) approach, as well as Dinkelbach's method (DK) were compared under the perspective of performance-complexity tradeoff. The findings reported in the previous papers assume that there are no impact of queuing issues on the optical network convergence and performance. To highlight this important aspect, in [13] the authors carried out a review on the role of the queuing theory-based statistical models in wireless and optical networks.

The PRMSA is an NP-hard problem, which can be decomposed into several sub-problems with lower complexity, e.g.: PA, routing; spectrum assignment; and others [21], [25], [36]. Between them, the PA sub-problem is an important procedure: to combat the main impairments of the EONs, including the amplified spontaneous emission (ASE) and non-linearities interference (NLIs); to guarantee QoT in dynamic scenarios, minimizing the waste of resources during the network's lifetime; to increase the network capacity; to limit the power budged in the sense of maximizing the energy-efficiency (EE); to mitigate the effects caused by fluctuations in the amplifiers. Analytical and heuristic methods have seen proposed in the sense of the better performance and complexity trade-off [1]–[6], [10]–[15], [33]. In [18], the hurricane searches optimization (HSO) was proposed as a candidate heuristic for the solution of NP-hard problems with large-scale, but it has not seen investigated in optical scenarios. Recently, the HSO was considered as a promising alternative algorithm for solving problems in practical large-scale power systems [19].

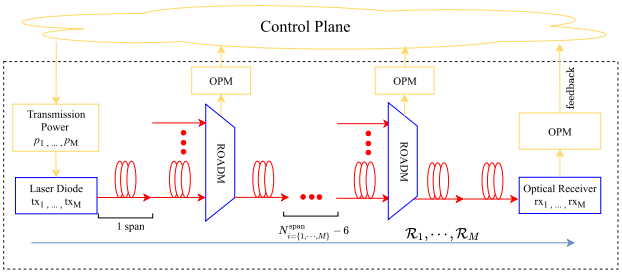

FIGURE 1. Elastic optical network topology highlighting the chaos heuristic-based power control block composed by a power allocation based on chaotic hurricane search optimization (PA-CHSO) scheme based on QoT estimation.

In this context, the contributions of this work include: a) proposing an effective, efficient PA strategy based on the HSO and its variation based on the insertion of a chaotic map, named PA-HSO and -CHSO, respectively; b) investigating systematically the input parameter optimization (IPO) for both PA algorithms, aiming at improving the performance-complexity tradeoff of the proposed algorithm; c) validating both PA algorithms for different realistic EON channel conditions, i.e., non-perfect monitoring of the OPMs, channel ageing effects, dynamical scenarios, including power instability, particularly in EONs. Moreover, comparisons have been performed assuming a convex optimization through the gradient descent (GD) [14], [15].

Channel estimation is evaluated in terms of Qot parameters, which are obtained from OPMs. OPMs measure the connection status and update the PA algorithms as illustrated in Fig. reffig:1. Thus, PA algorithms perform dynamic power control. To corroborate the effectiveness and efficiency of the proposed resource allocation strategy in EONs, it is evaluated: normalized mean square error (NMSE); convergence; power penalty (PP); probability of success; CC; and performance-complexity tradeoff.

II. PROPOSED SCHEME

The proposed scheme utilizes the information collected from the OPMs to control dynamically the level of the launch power of the lightpaths. The power adjustment considers the QoT inaccuracies, equipment ageing, inter-channel interference, as well as the variation of the optical power dynamics. Differently of the others approaches based on intelligent systems [14], it is not necessary the training phase and the proposed scheme can be performed in near-real time. In addition, the power budget is determinate in the planning stage of the network and margins are included [2], [4] and the proposed scheme will act during the regular operation of the EON. For the proposed scheme it is considered that the lightpaths were previously established from the resource allocation algorithms associated with route, modulation, bandwidth and spectrum.

The proposed scheme continuously update the transmitter launch power for each lightpath in response to dynamic OPMs information, it is considered a communication delay

between the OPMs in the receiver node, control plane and transmitter adjustment. This process can encompass the delay related to the duration of the OSNR estimation in the OPM, the control message transmission duration, the processing time, the actuation phase in the transmitter and the round-trip delay. In this sense, considering the current technology, each algorithm updating can be estimated in 100 ms or less [4]. Therefore, the time needed to close the loop related to the signal latency and the other operations needed for controlling the transmitted power is assured.

The proposed PA algorithm utilizes the chaotic hurricane, which is a new hybrid algorithm based on the hurricane search optimization (HSO) associated with probability distribution from the chaotic maps instead of uniform distribution of the traditional HSO. The objective is obtain an algorithm with balance between the exploration (diversification) and the exploitation (intensification) to improve the algorithm capability to escaping of the local solutions and the amelioration of the velocity of the convergence without affecting the quality of the algorithm solutions [16], [17].

The HSO is a metaheuristic algorithm for global optimization considering single-objective [18] and multi-objective [19] optimization problems, inspired by natural phenomena on the hurricanes behavior, where wind parcels move in a spiral course moving away from a low-pressure zone called the eye of the hurricane. These wind parcels search for possible new eye position, which represents a lower pressure zone to find out the optimal solution. The performance is very competitive compared to others metaheuristics optimization algorithms, such as gravitational search algorithm (GSA) and PSO. Although there is a variety of optimization algorithms, the development of new optimization algorithms have been motivated by the no free lunch (NFL) theorems for optimization, which have proved that an universally efficient optimization algorithm does not exist. Moreover, the particularities and characteristics of the optimization problem strongly affects the capacity of the optimization algorithm to finding the optimal solution in global optimization problems [18]. Herein, it is important investigate several distinct optimization algorithms for different optimization problems considering the related aspects. In addition, the application of chaos theory alone or jointly with other algorithms such as ant colony algorithm (ACO) [16], firefly algorithm (FA) [20] and PSO [17] have improved the optimization algorithms. Chaos presents a non-repetitive nature that increase the random search characteristics of the optimization methods, as well as increases the ability to get away from local solutions. In general, chaotic maps based on the complex behavior of a nonlinear deterministic system are utilized to optimization goal.

III. SYSTEM MODEL AND PROBLEM FORMULATION

The EON physical layer is composed by transmitters with adjustable modulation format, SNR rate and level of launch power, an erbium-doped fiber amplifier (EDFA) per span, ROADMs and receivers with digital signal processing capability to compensate the dispersion effects. The ROADMs present equalization to compensate undesired spectrum tilting due to EDFAs. In addition, the EDFAs operate in an automatic gain controlled (AGC) mode according to each ROADM to achieve spectral tilt correction. A connection between ith and jth node, i.e., $\mathcal{N}(i,j)$, is called communication link. The ith link from ith channel is formed by N_i^{span} spans, being each span formed by: a fiber length L in Km; and an EDFA. The lightpaths are represented as Nyquist wavelength division multiplexing (WDM) super-channels with bandwidth

$$\Delta f_i = \frac{\xi_i}{c_i}, \quad i = 1, \ldots, M, \tag{1}$$

where ξ_i is the traffic demand data rate (Gbps) of the ith channel, M is the number of channels and c_i is the spectral efficiency defined by modulation format of the ith channel, Table 1. The $\gamma^*_{\text{B2B},i}$ is the back-to-back signal-to-noise ratio target for the ith channel required to achieve error-free considering forward-error-correction (FEC) codes with bit-error-rate requirement of $b^* = 4 \cdot 10^{-3}$.

TABLE 1. Modulation format, spectral efficiency and SNR.

Modulation format	Spectral Efficiency c_i (bps/Hz)	γ^*_{B2B} (dB)
PM-BPSK	2	5.50
PM-QPSK	4	8.50
PM-8QAM	6	12.50
PM-16QAM	8	15.15
PM-32QAM	10	18.15
PM-64QAM	12	21.10

Hence, to obtain an appropriate QoT, the effective back-to-back signal-to-noise ratio for the channel i ($\gamma_{\text{B2B},i}$) must be $\gamma_{\text{B2B},i} \geq \gamma^*_{\text{B2B},i}$. This formulation can be defined as a problem of residual margin (RM). The RM in the ith channel can be defined as [14]:

$$\Psi_i = \frac{\gamma_{\text{B2B},i}}{\gamma^*_{\text{B2B},i}}, \tag{2}$$

while the RM in vector form is represented as $\Psi = [\Psi_1, \Psi_2, \cdots, \Psi_M]^{1\times M}$. The concept of residual margin Ψ in WDM systems can be formulated as an optimization problem, which the objective is to minimize the RM of all the M WDM channels in the sense of $\Psi^* = [1, \cdots, 1]^{1\times M}$, while guaranteeing the QoT.

Such RM optimization problem can assume an optical network topology as static in a short-time due to the multi-stage traffic demand. Therefore, the optimization problem reduces to the efficient power assignment problem [5]:

$$\begin{aligned}
&\underset{\mathbf{p}\in\mathbb{R}^M}{\text{minimize}} && J(\mathbf{p}) = \textstyle\sum_{i=1}^{M} p_i \;=\; 1^T\mathbf{p} \\
&\text{s.t.} \quad \text{(C.1)} && \gamma_{\text{B2B},i} \geq \gamma^*_{\text{B2B},i} \qquad i = 1, \ldots, M \\
&\qquad \text{(C.2)} && \xi_i \geq \xi_i^{\min} \qquad i = 1, \ldots, M \\
&\qquad \text{(C.3)} && p_{\min} \leq p_i \leq p_{\max} \qquad i = 1, \ldots, M
\end{aligned} \tag{3}$$

where $\mathbf{p} = [p_1, p_2, \cdots, p_M]^T$ is the optical power vector and p_i the transmitted optical power for the ith lightpath, subject to the constraints related to power budget and SNR required to achieve QoT [3]; moreover, $\xi_i^{\min}$ is the requirement minimum bit-rate, $p_{\min}$ and $p_{\max}$ is the minimum and maximum value considered as allowable transmitted power, respectively.

The quality of the RM optimization attained by different methods can be evaluated via the Euclidean distance between Ψ and Ψ^*. Mathematically, this is expressed as:

$$\begin{aligned} &\underset{\mathbf{p}\in\mathbb{R}^M}{\text{minimize}} \quad J_1(\mathbf{p}) = \|\Psi^* - \Psi\|_2 \\ &\text{s.t.} \quad \text{(C.1), (C.2), (C.3) of eq. (3).} \end{aligned} \tag{4}$$

From eq. (3), the problem in the original form is not convex. Therefore, it do not guarantee the minimum global of Ψ applying nonlinear programming (NLP), because can to result in a solution that is far from global solution Ψ^*. In this sense, heuristic evolutionary optimization methods, such as the HSO, have the advantage of achieving in a polinomial processing time an high quality solution, which is not necessary the optimum solution. For comparison purpose, in the numerical results it will be evaluated descent gradient (GD) proposed [15] with convex formulation [14]. The first constraint (C.1) from eq. (3) is based on a Gaussian noise (GN) model to establishment the QoT in the lightpath [21], [22].

For the proposed evaluation scenario in Fig. 1, it is considered that the ith lightpath characteristics such as modulation formats, routes, and spectral orderings of all the connections were previously determined, and it includes the *design margin* $M_d(\tau)$ due to the QoT model inaccuracies and ageing margin of the transponder $M_t(\tau)$ on its sensitivity, modeled as a function of time τ. Basically, the design margin $M_d(\tau)$ is included to overcome the GN model inaccuracies and avoid the EON operating at the limit. $M_d(\tau)$ decreases along with the time τ (in years), since a better EON knowledge is obtained by increasing of τ [4], [7], [9], [25].

Hence, the $\gamma_{\text{B2B},i}$ for the ith channel is modeled as:

$$\gamma_{\text{B2B},i}(\tau) = \gamma_i(\tau) - M_d(\tau) - M_t(\tau) \tag{5}$$

where each parameter from eq. (5) can be modeled as a linear or nonlinear function of time τ [4]. Herein, we have adopted the following linear function of τ:

$$M_t(\tau) = \frac{M_t(\tau_{\text{end}}) - M_t(\tau_0)}{\Delta\tau} \cdot \tau \tag{6}$$

where $M_t(\tau_{\text{end}})$ and $M_t(\tau_0)$ are the transponder margin for End-of-Life (EoL) and Begin-of-Life (BoL) time, respectively, while $\Delta\tau = \tau_{\text{end}} - \tau_0$ is the network's lifetime. Besides, the first term $\gamma_i(\tau)$ assumes GN model, while includes the linear and nonlinear noise effects for the ith channel [21]:

$$\gamma_i(\tau) = \frac{p_i}{p_i^{\text{ASE}}(\tau) + p_i^{\text{NLI}}(\tau)} \tag{7}$$

where $p_i^{\text{ASE}}(\tau)$ is the power of the amplified spontaneous noise (ASE) noise and $p_i^{\text{NLI}}(\tau)$ is the power of the non-linear interference (NLI) noise.

The power of the ASE noise is given by [4], [21]:

$$p_i^{\text{ASE}}(\tau) = h \cdot \nu \cdot F \cdot \Delta f_i \cdot \left(\sum_{e=1}^{N_i^{\text{ROADM}}} (A_{e,i}^{\text{ROADM}} - 1) + \sum_{e=1}^{N_i^{\text{span}}} (A_{e,i}^{\text{span}} - 1) \right) \tag{8}$$

where h is the Planck's constant, ν is the carrier frequency, F is the noise figure of the edfa, N_i^{span} and N_i^{ROADM} are the number of span and ROADM of the ith user, respectively. $A_{e,i}^{\text{ROADM}}(\tau)$ and $A_{e,i}^{\text{span}}(\tau)$ are the losses of the eth span and eth ROADM from the ith user, respectively, being the last given by:

$$A_{e,i}^{\text{span}}(\tau) = L_{e,i} \cdot \alpha(\tau) + c_{e,i} \cdot c_{\text{loss}}(\tau) + s_{e,i} \cdot s_{\text{loss}}(\tau) \tag{9}$$

where for the eth span of the ith user, the $L_{e,i}$ is span length; $c_{e,i}$ is connection number, and $s_{e,i}$ is the splice number; while $\alpha(\tau)$, $c_{\text{loss}}(\tau)$ and $s_{\text{loss}}(\tau)$ can be modeled as functions of time, representing the fiber attenuation, the connector's loss and the splice loss, respectively [4].

The power of the NLI noise results of the self- and cross-channel interference, SCI and XCI, respectively. It is given by:

$$p_i^{\text{NLI}}(\tau) = \underbrace{\frac{3\zeta^2}{2\pi\alpha(\tau)|\beta_2|} \sinh^{-1}\left(\frac{\pi^2|\beta_2|}{2\alpha(\tau)}\Delta f_i^2\right) N_i^{\text{span}}}_{\eta_i'(\tau)} \cdot p_i^3 + \underbrace{\frac{6\zeta^2}{\alpha^2(\tau)} \sum_{j\neq i} \frac{\alpha(\tau)}{4\pi|\beta_2|} \log\left|\frac{|f_i - f_j| + \Delta f_j/2}{|f_i - f_j| - \Delta f_j/2}\right| N_i^{\text{span}}}_{\eta_i''(\tau)} \cdot p_i \cdot p_j^2 \tag{10}$$

where $\eta_i'(\tau) + \eta_i''(\tau)$ defines the non-linear factor of the transmitted signal spectrum of the ith channel, denoted as η_i. ζ is the non-linear parameter, β_2 is the group velocity dispersion and p_j is the power of jth interfering channels. Therefore, it can be obtained a bit error rate (BER) expressed as a function of the SNR, which takes into account the baud-rate, FECs limit BER and the modulation format of the ith channel [23], [24], as follows:

$$b_i = \vartheta(\gamma_{\text{B2B},i}(\tau)) \tag{11}$$

where the function $\vartheta(\cdot)$ is defined by modulation format [4].

The QoT prediction consists of developing a systematic procedure for the evolution of the vector $\mathbf{p}$ in order to reach the optimum value $\mathbf{p}^*$, based on the $\gamma_{\text{B2B},i}(\tau)$, $\gamma_{\text{B2B},i}^*$, b_i, b_i^* values. Theses values are monitored by OPMs at add, through and drop node by channel estimation and reported to the control plane to guarantee the QoT. The channel estimation quality is affected by three main assumptions:

1) non-perfect monitoring of the OPMs considering their limited accuracy due to channel impairments (linear and nonlinear effects) and the receiver architecture, as well the noise measurement and peaks occurrence caused by polarization mode dispersion (PMD) effects [2], [4], [6], [25], [26]. Theses uncertainties

can be modeled as a random variable δ_i added to the $\gamma_{\mathrm{B2B},i}$,which follows a Log-Normal distribution $\mathcal{LN}(\mu,\sigma)$. Therefore, the estimated $\gamma_{\mathrm{B2B},i}$ can be modeled by [6]:

$$\widehat{\gamma}_{\mathrm{B2B},i}(\tau)=\gamma_{\mathrm{B2B},i}(\tau)(1+\delta_i)\quad \forall_i,\ \delta_i\sim\mathcal{LN}(\mu,\sigma) \tag{12}$$

2) ageing resulting from increases fiber losses due to splices to repair fiber cut, detuning of the lasers leading to misalignment with optical filters in the intermediate and add/drop nodes. These values can be modeled by eqs. (8)-(9) as function of time τ, assuming the parameter values based on Begin-of-life (BoL) and End-of-life (EoL) in an elastic optical network.
3) power instability resulting from power variations due linear and nonlinear effects associated to the optical fiber and coupling, both influenced by traffic variation, network topology, physic aspects of the EDFA and ROADM at add/drop channel, and unpredictability of fast time-varying penalties, such as polarization effects. Theses values can be modeled as a power perturbation in the input power of the ith user:

$$p_i^{\circ}[n]=\mathrm{pert}[n]+10\log_{10}\frac{p_i}{10^{-3}}\qquad[\mathrm{dBm}] \tag{13}$$

where the power perturbation function is modeled as

$$\mathrm{pert}[n]=A^n\cdot\sin(n\pi/2), \tag{14}$$

with A^n being the peak of the perturbation in [dB], n is a discrete-time index, and p_i the nominal transmitted power for the ith lightpath. This model assumes power fluctuations propagation across the network nodes [6].

The full knowledge of the QoT parameters during the estimation of the ith channel increases reliability and enables design solutions considering the $\mathbf{p}^*$ for different bit rates requirement in the lightpath. In this sense, mixed line rates (MLR) networks have focused on optimum launch power, obtaining suitable cost minimization [27], combined to the maximization of the number of established connections [10], while reducing the transponder cost [28] and improving the launch power versus regenerator placement tradeoff [29]. However, when the QoT parameters for the ith channel is not known perfectly, PP occurs, being modeled as:

$$\bar{p}_i(n)=10\cdot\log\left(\frac{p_i(n)}{p_i^*}\right)\qquad[\mathrm{dB}] \tag{15}$$

where the p_i^* value is defined considering the perfect knowledge of the QoT parameters [5]. Negative values of $\bar{p}_i$, i.e, $\bar{p}_i^{(-)}$, mean that the measured BER did not reach the p^*; while positive values of $\bar{p}_i$, i.e, $\bar{p}_i^{(+)}$, mean that the b^* is reached with energy waste. Therefore, for availability of the ith lightpath, the margins (m_i) should satisfying the condition of $m_i\geq\bar{p}_i^{(-)}$.

In context of margins, in [8] a system margin (SM) is adjusted by a ML based on the maximum-likelihood principles to improve the QoT prediction of new lightpaths. The predict parameters can provided more accurate QoT of not-already-established lightpaths compared to the limited amount of information available at the time of offline system design. In [11] is proposed a ML-based classifier to predict if the candidate lightpath presents suitable bit error rate (BER) considering the traffic volume, modulation format, lightpath total length, length of its longest link, and number of lightpath links. To train of the ML classifier is based on the OPMs or in the BER simulation, which is utilized in the absence of real field data. In [14] is performed the optimization of transmitted power to maximize minimum margin and to maximize a continuously variable data rate. The Gaussian noise nonlinearity model is utilized to expresses the SNR in each channel as a convex function of the channel powers. Convex optimization is performed with objectives of maximizing the minimum channel margin.

Therefore, the progress in the network planning, design and active operation control has become margins an important resource to be optimized [2], [4]. In this sense, the margin in each lightpath should be as little as possible to ensure guarantee reliable optical connectivity. The reducing of the excess margin can be utilized to increase the maximum transmission distance, reduce the number of regenerators, as well as postpone the installation of more robust transponders than are closely necessary in the beginning of the network operation [25]. Several efforts have been made to become the margins variable and adjustable to increase the network capacity and decrease the costs of the network implantation and operation [1]- [6]. In this sense, the determination of the level of transmitted power is performed in the planning stage of the network and a SM is included considering the uncertainties of the OPMs measurements and optical power dynamics [7], [21].

IV. PA SCHEMES

In this section, the PA-HSO and -CHSO schemes are proposed for PA in EONs. Firstly, the recently proposed heuristic HSO [18] is revisited in the sequel, and modifications are implemented to solve suitably the PA-EONs optimization problem. Hence, the original HSO is modified further, with the insertion of a chaotic map [16], [17]. Moreover, the PA-GD in [14], [15] are applied aiming at comparing the complexity-performance tradeoff with the proposed PA methodology. Indeed, the PA-GD is assumed as an analytical method, which result in a global optimum solution in a cost of high complexity.

A. PA-HSO

In the HSO, the eye (lower pressure zone) is related to the best solution of the hurricane structure and can be represented at nth iteration by the matrix $\boldsymbol{P}[n]=[\mathbf{p}_1[n],\mathbf{p}_2[n],\cdots,\mathbf{p}_K[n]]\in\Re^{M\times K}$, which is composed by K wind parcels, defined as $\mathbf{p}_K[n]=[p_{k,1}[n],\ p_{k,2}[n],\ \cdots,\ p_{k,M}[n]]^{\mathrm{T}}\in\Re^{M\times 1}$, while the hurricane eye is the best candidate vector solution at nth iteration, written as $\hat{\mathbf{p}}[n]=[\hat{p}_1[n],\ \hat{p}_2[n],\ \cdots,\ \hat{p}_M[n]]^T\in\Re^{M\times 1}$. Besides, K is composed by wind parcels factor N_w and M channels, resulting

$K = M \cdot N_w$. The pressure function at the nth iteration for the hurricane eye $p_{\hat{\mathbf{p}}}[n]$, as well as for the candidate solutions $p_{\mathbf{P}_k}[n]$ is measured by a fitness function in eq. (4), *i.e.*, pressure($\hat{\mathbf{p}}[n]$) $= J_1(\hat{\mathbf{p}}[n])$.

The kth wind parcel on the nth iteration moves around the eye according to:

$$r_k[n](\theta_k[n]) = r_0 \cdot \exp\left(z_k[n] \cdot \theta_k[n]\right), \tag{16}$$

where $r_k[n]$ and $\theta_k[n]$ are respectively the radial and angular coordinate of the power increasing of the kth wind parcel at the nth iteration. r_0 is the initial value of r_k. And, $z_k[n]$ is the rate of the increase of the spiral at nth iteration, which is defined by a random variable with uniform distribution, i.e., $z_k[n] \sim U \in \mathcal{U}[0, 1]$. Indeed, the behavior of the kth wind parcel in the nth iteration follows a logarithmic spiral pattern. The system evolves looking for a lower pressure zone (new eye position) in the search space. Once a new lower pressure is discovered, its position ($\mathbf{P}_k$) becomes the eye ($\hat{\mathbf{p}}$) and the process start over and the process start over again [18].

From eq. (16) and (20), the power updating of two consecutive channels associated to the kth wind parcel at the nth iteration is given by:

$$\begin{aligned} p_{k,i}[n] &= r_k(\theta_k[n])\cos(\theta_k[n]) + \hat{p}_i[n] \\ p_{k,i+1}[n] &= r_k(\theta_k[n])\sin(\theta_k[n]) + \hat{p}_{i+1}[n] \end{aligned} \tag{17}$$

where $i = (k \bmod h) + 1$ corresponds to the ith channel from the kth parcel updating, that represents K wind parcels. Each group is denoted by $\mathcal{G}_i$, representing the power updating of two specific channels from $\mathbf{p}_k$, as in eq. (17), resulting $\mathbf{p}_k \subset \mathcal{G}_i$.

The $\theta_k[n]$ updating from eq. (17) is defined by concept of velocity variation of the kth wind parcel in the nth iteration, which is given by:

$$\begin{aligned} \omega_k^{\mathrm{WP}}[n] &= \omega_{\max}^{\mathrm{WP}} \cdot \left(\frac{r_k[n]}{p_{\max}}\right) \quad \text{if} \quad r_k[n] < p_{\max} \\ \omega_k^{\mathrm{WP}}[n] &= \omega_{\max}^{\mathrm{WP}} \cdot \left(\frac{p_{\max}}{r_k[n]}\right)^{z_k[n]} \quad \text{if} \quad r_k[n] > p_{\max} \end{aligned} \tag{18}$$

where $\omega_k^{\mathrm{WP}}[n]$ is a tangential velocity of the kth wind parcel at nth iteration, $\omega_{\max}^{\mathrm{WP}}$ is the maximum tangential velocity adopted for all the wind parcels, $z_k[n]$ performs $\omega_k^{\mathrm{WP}}[n]$ fit at nth iteration [18]. Thus, the $\theta_k[n]$ updating at the nth iteration is given by:

$$\begin{aligned} \theta_k[n] &= \theta_k[n] + \omega_k^{\mathrm{WP}}[n] \quad \text{if} \quad r_k[n] < p_{\max}, \\ \theta_k[n] &= \theta_k[n] + \omega_k^{\mathrm{WP}}[n]\left(\frac{p_{\max}}{r_k[n]}\right)^{z_k[n]} \quad \text{if} \quad r_k[n] > p_{\max}, \end{aligned} \tag{19}$$

where ω_k^{WP} is assumed as a fixed value $\forall k$, because $p_{\max}$, $r_k[n]$ and $z_k[n]$ are sufficient to update the kth wind parcel.

In addition, the initial power vector of the PA-HSO is defined as $\mathbf{p}_0$ while the component $p_{k,i} \in [p_{\min};\ p_{\max}]$. Therefore, when $p_{k,i} \notin [p_{\min};\ p_{\max}]$, the function $\varphi(p_{k,i})$ is true; thus, the initial and current angular coordinates of the kth wind parcel, $\theta_k[1]$ and θ_k, respectively, must be updated as:

$$\theta_k[1] = z_k[1] \qquad \text{and} \qquad \theta_k = 0.$$

The stopping criterion is defined by the number of iterations N_f. A pseudo-code for the PA-HSO is described in Algorithm 1.

Algorithm 1 PA-HSO or -CHSO – Power Allocation Based on the Traditional or Chaotic Hurricane Search Optimization

Input: N_f, K, ω^{WP}, r_0, $r_{\max}$, $\theta_k[1]$, $p_{\min}$, $p_{\max}$, $\theta_k[n] = 0$, $\mathbf{p}_0$;
Output: $\hat{\mathbf{p}}[n]$;

```
1:  p̂[n] = p0;
2:  for n = 1 to Nf
3:  pp̂[n] = pressure (p̂[n]);
4:    for k = 1 to K
5:      (a) rk[n] = r0 · exp(θk[n] · zk[n]);
6:      (b) pk[n] = p̂[n];
7:      (c) i = (k mod h) + 1;
8:      (d) pk,i[n] = ri · cos(θk[1] + θk[n]) + p̂i;
9:      (e) pk,i+1[n] = ri · sin(θk[1] + θk[n]) + p̂i+1;
10:     (f) ppk[n] = pressure (pk[n]);
11:     (g) if φ(pk,i) or φ(pk,i+1);
12:           θk[1] = zk[n] · 2π;
13:           θk = 0;
14:         else if ppk[n] < pp̂[n]
15:           e = pk;
16:           pp̂[n] = pressure (p̂[n]);
17:         else
18:           if rk[n] < pmax;
19:             θk[n] = θk[n] + ω;
20:           else
21:             θk[n] = θk[n] + ω (rmax / rk[n])^zk[n];
22:           end
23:         end
24:   end
25: end
```

B. PA-CHSO

The PA-CHSO and -HSO algorithm are similars. The updating of $z_k[n]$ is the unique difference between them. As described in subsection IV-A, the PA-HSO assumes $z_k[n]$ as a random variable with uniform distribution. However, aiming to escape of local minimum and to diversify the candidate solutions, the PA-CHSO assumes $z_k[n]$ as a random variable assigned by a chaotic mechanism [16], [17]. Such chaotic logistic map is related to the dynamics of the biological population with the chaotic distribution features and it is obtained by the recursive equation:

$$z_k[n+1] = \mu \cdot z_k[n](1 - z_k[n]), \tag{20}$$

where $z_k[n] \in [0, 1]$ is the chaotic variable and μ is the control parameter in the range $0 < \mu \leq 4$ [16], [17].

The assumed $z_k[n]$ values brings randomness to the search step when compared with uniform distribution. Therefore, the same PA-HSO algorithm can be adopted, i.e., Algorithm 1, but $z_k[n]$ is updated by the eq. (20).

C. PA-GD

The PA-GD algorithm is based on the outline of a general GD method [14], [15], which defines a descent direction $\Delta_{\mathbf{p}}$ and a suitable step size selection using backtracking line search method (from Algorithm 9.1 and 9.2 in Ref. [15]). Here, $\Delta_{\mathbf{p}}$ is normalized by $||J_1(\mathbf{p})||$. Summarizing, the main parameters are the number of iterations (N_f^{GD}) from Algorithm 9.1 and the number of iterations from the backtracking search (N_{bt}^{GD}) [15]).

D. INPUT PARAMETERS OPTIMIZATION (IPO)

In this subsection, two input parameter optimization (IPO) strategies are proposed: IPO based on the golden-section (GS), which is a numerical method for uni-modal optimization, hereafter named IPO-GS [35]; and the IPO based on the conditional probability of success (CPoS), which is a empirical method based on the combination of the input parameters inside theirs range, hereafter named IPO-CPoS. Firstly, the IPO-GS and IPO-CPoS optimize the input parameters that affect dramatically the performance. After, the IPO-CPoS optimizes the input parameters that affect dramatically the CC. The IPO-GS is not adopted to optimize the CC, because it increases a larger CC to minimize the objective, i.e., eq. (3). More details about them are described below.

Algorithm 2 IPO Procedure: PA-CHSO and -HSO

Input: N_{lps}, tol_{r_0}, $\mathrm{tol}_{\omega}^{\mathrm{WP}}$, $p_{\min}$, $p_{\max}$, $\omega_{\min}^{\mathrm{WP}}$, $\omega_{\max}^{\mathrm{WP}}$, g_s, N_f, K, ω^{WP}, $r_{\max}$, $\theta_k[1]$, $p_{\min}$, $p_{\max}$, $\theta_k[n]=0$, $\mathbf{p}_0$;
Output: ω^{WP}, r_0;
1: **for** $n_{\mathrm{lps}} = 1$ to N_{lps}
2: *if* $n_{\mathrm{lps}} = 1$
3: (a) $r_l = \log(p_{\min})$;
4: (b) $r_u = \log(p_{\max})$;
5: *else*
6: (a) $I_{n_{\mathrm{lps}}} = \frac{\min(|r_0 - r_l|, |r_0 - r_u|)}{(0.5 g_s^{(n_{\mathrm{lps}}-2)})}$
7: (b) $r_l = \log(r_0) - I_{n_{\mathrm{lps}}}/2$;
8: (c) $r_u = \log(r_0) + I_{n_{\mathrm{lps}}}/2$;
9: **end**
10: keeps ω^{WP} fixed;
11: **while** $|r_l - r_u| < \mathrm{tol}_{r_0}$
12: *if* $\mathcal{E}_1 < \mathcal{E}_2$
13: (a) $r_u = \hat{r}_2$;
14: (b) $\hat{r}_2 = r_u - g_s(r_u - r_l)$;
15: **else** $\mathcal{E}_1 > \mathcal{E}_2$
16: (a) $r_l = \hat{r}_1$;
17: (b) $\hat{r}_1 = r_u + g_s(r_u - r_l)$;
18: **end**
19: **end**
20: $r_0 = (r_l + r_u)/2$;
21: executes ω^{WP} optimization analogous to lines **2** to **22**;
22: **end**

1) IPO-GS

The framework of the IPO-GS is similar to the systematic proceeding proposed in [32], in which only the main input parameters that affect dramatically the performance of the PA algorithms are optimized, i.e., for the PA-HSO and -CHSO are r_0 and ω^{WP}. After that, the input parameters directly related to the algorithm's complexity are optimized regarding the performance-complexity tradeoff, i.e.; for the PA-HSO and -CHSO are K and N_f.

The IPO-GS is presented for the PA-HSO, but it also is applied on the PA-CHSO. The IPO-GS procedure consists of two steps: a) keep ω^{WP} fixed and optimizes r_0; b) r_0 (from first step) is hold fixed while ω^{WP} value is optimized. The optimized input parameter values are found by golden-section search method, which finds the minimum of an objective function by successively narrowing the range of values inside feasible range; in other words, it estimates the maximum and minimum values of the input parameter until the best value of r_0 and ω^{WP} have been found. Both optimization input parameter procedure adopt the same steps; for this reason Algorithm 2 details only the r_0 optimization.

From Algorithm 2, analogous the golden section search algorithm [35], the golden-section value is $g_s = \frac{1+\sqrt{5}}{2}$, while $r_{\min}$ and $r_{\max}$ are minimum and maximum value of r_0, respectively; N_{lps} is the number of loops for reduction of the interval $I_{n_{\mathrm{lps}}}$, $\hat{r}_1$ and $\hat{r}_2$ are the intermediates points; $|r_{\max} - r_{\min}| < \mathrm{tol}_{r_0}$ is the stopping criterion of r_0; tol_{r_0} is the tolerance adopted; $\omega^{\mathrm{WP}} \in [\omega_{\min}^{\mathrm{WP}}; \omega_{\max}^{\mathrm{WP}}]$ is the parameter keeps fixed; and log operator performs the normalization of r_0 range. $\mathcal{E}_1$ and $\mathcal{E}_2$ are given by the $\mathbb{E}[J_1(\hat{\mathbf{p}}[n])]$, assuming $r_0 = 10^{(\hat{r}_1)}$ and $r_0 = 10^{(\hat{r}_2)}$, respectively, while $\hat{\mathbf{p}}[n]$ is calculated via Algorithm 1. N_r realizations are adopted to measure $\mathbb{E}[J_1(\hat{p})[n]]$. In this context, the ω^{WP}, c_1 and c_2 optimization are obtained by replacing the variable r_0 by them.

2) IPO-CPoS

The IPO-CPoS re-optimizes the performance input parameter to corroborate with the IPO-GS. For each PA algorithm, i.e., PA-HSO or -CHSO, it assumes final values from the IPO-GS, i.e, ω^{WP} and r_0, so it fixes the parameter of lower impact, i.e., ω^{WP}, and re-optimizes the other, i.e., r_0. The r_0 parameter has higher impact than the ω^{WP}, because the power increasing granularity is given by it. In this context, the IPO-CPoS measures the probability of M channels to achieve the b^* in the n iteration with the lower energy waste given n and r_0, denoted by $\mathcal{P}s_1$.

The $\mathcal{P}s_1$ formulation follows the RM concept discussed in eq. (2). Then, given r_0 and n, it can be defined as the probability of M-users to satisfy two conditions: **i)** $\Psi_i \geq \Psi^* - \Lambda_1$, where Λ_1 assures the b^*; **ii)** $\Psi_i \leq \Psi^* + \Lambda_2$, where

Λ_2 assures the b^*. In this context, $\mathcal{P}s_1$ is given by:

$$\mathcal{P}s_1 \triangleq \Pr[\Psi^* - \Lambda_1 \leq \Psi \leq \Psi^* + \Lambda_2 \,|r_0, n]. \quad (21)$$

$\mathcal{P}s_1$ is evaluated over an average behavior of N_r realizations and its target value is defined as $\mathcal{P}s^*$.

After optimizing the performance input parameters, those that dramatically affect the complexity of the algorithm are also evaluated, i.e., for the PA-HSO and -CHSO, N_f and K. Therefore, analogous to the $\mathcal{P}s_1$, the optimization of theses parameters is modeled as:

$$\mathcal{P}s_2 \triangleq \Pr[\Psi^* - \Lambda_1 \leq \Psi \leq \Psi^* + \Lambda_2 \,|K, N_f, r_0, \omega^{\text{WP}}]. \quad (22)$$

$\mathcal{P}s_2$ is evaluated over an average behavior of N_r realizations and its target value is defined as $\mathcal{P}s^*$. There is a set of infinite number of pair combinations $(K;\ N_f)$ that found the CPoS, defined as $\mathcal{P}s_2 \geq 0.94$. Hence, the pareto frontier (PF) can be obtained. Here, the PF is composed by all success points $(K^*;\ N_f^*)$ assumed as reliable and viable. Mathematically, all the success points $(K;\ N_f)$ is defined by the set

$$\mathcal{V} = \{K \in \mathcal{K},\ \text{and}\ N_f \in \mathcal{N}_f\} \ |\ \mathcal{P}s_2 \geq \mathcal{P}s^*,$$

while the PF subset $\{(K_\iota^*, N_{f_\iota}^*)\}$ can be defined as:

$$\forall\,(K;\ N_f) \in \mathcal{V} \ |\ \forall N_{f_i},$$
$$K_\iota^* = \min(N_{f_i} \cdot K_j \,|\, K_j \geq K_{\iota-1}^*) \ \text{and}\ N_{f_\iota}^* = N_{f_i} \quad (23)$$

where all $(K_\iota^*;\ N_{f_\iota}^*)$ result of the increasing of $i = [1, \cdots, N_{N_f}]$ and $j = [1, \cdots, N_K]$, that represent the decreasing of K and N_f, respectively, with $N_{N_f} = |\mathcal{N}_f|$ and $N_K = |\mathcal{K}|$.

In this context, the performance-complexity tradeoff of the input parameters also is evaluated, e.g., ω^{WP}, r_0, K and N_f for the PA-CHSO or -HSO. Mathematically, it can be modelled as:

$$\min_{K,N_f} \left(\mathcal{C}(N_f, K) | \mathcal{P}s_2 \geq P_s^*, r_0, \omega^{\text{WP}}\right) \quad (24)$$

where $\mathcal{C}(\cdot)$ is the CC for the PA-CHSO or -HSO. The feasible solutions result in a Pareto front, which is given by the pairs (K, N_f).

E. Performance AND COMPLEXITY Analysis

The metrics for performance and CC analysis and tradeoff between them are presented. These metrics are used to measure the quality of the PA algorithm solutions during their operations.

1) Performance Analysis

The quality of the PA algorithms is measured based on the normalized mean square error (NMSE), and maximum and minimum PP for M channels. Both are related to the optimal solution vector p^*. The NMSE in the nth iteration is given by:

$$\text{NMSE}[n] = \mathbb{E}\left[\frac{\|\hat{\mathbf{p}}[n] - \mathbf{p}^*\|^2}{\|\mathbf{p}^*\|^2}\right] \quad (25)$$

where $\mathbb{E}$ is the expectation operator and $\|\cdot\|$ is the Euclidean distance to the origin. And, the maximum and minimum PP assuming M channels in the nth iteration are given by $\bar{p}_{\max}^{(+)}[n] = \max\{\hat{\mathbf{p}}[n]\}$ and $\bar{p}_{\min}^{(-)}[n] = \min\{\hat{\mathbf{p}}[n]\}$, which are based on the eq. (15).

2) Complexity Analysis

The computational complexity (CC) is evaluated to measure the performance of the algorithms. Here, the CC is computed during the PA of each algorithm based on the floating-points operations (flop)s count, denoted as $\mathcal{C}$. $\mathcal{C}$ is affected by the number of active channels (M), by the size and number of routes, i.e., N_i^{ROADM} and N_i^{span}, which are related to measured SNR, from eq. (8), as well as by the number of iterations from algorithms N_f. The most relevant metric of CC is $\mathcal{C}$, because it does not depend on the machine, operating system, and programming structure and style.

$\mathcal{C}$ is evaluated for each PA algorithm as a function of the number of mathematical operations necessary to run until convergence. These operations include addition, subtraction, multiplication, division (or mod operator), natural logarithm, power or exponential and trigonometric functions, where each is assumed as one floating-points operation (flop). Logical (i.e., and, or) and comparison (i.e., if, else, else if, $\leq$, etc…) operations, and variable assignment were considered irrelevant time-consuming operations.

In this context, the $\mathcal{C}$ of each PA algorithm in the nth iteration is modeled. In case of the PA-HSO, from Algorithm 1 it is given by

$$\mathcal{C}^{\text{PA-HSO}} = 25N_f \cdot K + \\ +3 \cdot \left(19M^2 + 5M + \sum_{i=1}^{M}(N_i^{\text{ROADM}} + N_i^{\text{span}})\right) N_f \cdot K, \quad (26)$$

in case of the PA-CHSO, from Algorithm 1 and chaotic map in eq. (20), it is given by

$$\mathcal{C}^{\text{PA-CHSO}} = \mathcal{C}^{\text{HSO}} + 6N_f \cdot K \quad (27)$$

and, in case of PA-GD, from section IV-C, $\mathcal{C}_n$ is given by:

$$\mathcal{C}^{\text{PA-GD}} = N_f^{\text{GD}}(M^2 + 4M + 3) \\ + \left[19M^2 + 5M + \sum_{i=1}^{M}(N_i^{\text{ROADM}} + N_i^{\text{span}})\right] \\ \cdot \left[N_f^{\text{GD}}(5 \cdot N_{bt}^{\text{GD}} \cdot M + 5 \cdot M + 1)\right] \quad (28)$$

Asymptotically, the $\mathcal{C}$ of the PA-HSO, -CHSO and algorithms is of order of $\mathcal{O}(M^2)$, while $\mathcal{C}$ of the PA-GD is of order of $\mathcal{O}(M^3)$.

V. NUMERICAL RESULTS

In this section, the performance of the PA-CHSO and -HSO are analyzed and systematically compared. Section V-A presents network's scenario and parameters, while section V-B describes the input parameters optimization (IPO). Sections V-C and V-D analyse the PA performance

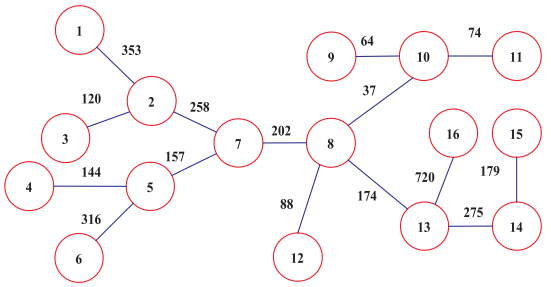

FIGURE 2. Adopted EON topology; distance in km.

TABLE 2. Channels features: Routes, distance, bit rate and modulation format.

Route	$\mathcal{S} \rightarrow \mathcal{D}$	Distance (km)	R (Gbps)	Modulation
$\mathcal{R}_1$	1 - 16	1707	100	PM-QPSK
$\mathcal{R}_2$	1 - 15	1441	100	PM-QPSK
$\mathcal{R}_3$	1 - 14	1262	100	PM-QPSK
$\mathcal{R}_4$	1 - 9	914	100	PM-QPSK
$\mathcal{R}_5$	3 - 14	1029	150	PM-8QAM
$\mathcal{R}_6$	3 - 13	754	150	PM-8QAM
$\mathcal{R}_7$	3 - 12	842	200	PM-16QAM
$\mathcal{R}_8$	6 - 10	712	200	PM-16QAM
$\mathcal{R}_9$	4 - 9	604	250	PM-32QAM
$\mathcal{R}_{10}$	5 - 11	470	250	PM-32QAM
$\mathcal{R}_{11}$	7 - 11	235	300	PM-64QAM
$\mathcal{R}_{12}$	7 - 10	313	300	PM-64QAM

for both PA-CHSO and conventional -HSO methods considering perfect and non-perfect channel estimation, respectively. CC assuming different system loading is discussed in section V-E. The numerical simulations were performed with MATLAB (version 7.1) in a computer with 32 GB of RAM and processor Intel Xeon E5-1650@ 3.5 GHz.

A. NETWORK PARAMETERS

Fig. 2 illustrates a virtual network topology for the transmission routes from source ($\mathcal{S}$) to destination ($\mathcal{D}$). The span length is 100 Km, channel spacing (Δf) of 50 GHz and guard band of 6 GHz. This topology was chosen to concentrate the routes $\mathcal{R}$ in some links, thus the effects of interference, as well as the effects of nonlinearities are more prominent. The EON transmission capability is in range of 100 to 300 Gbps. The routes and spectrum assignment procedure is out of the scope of this work, as these are considered to be stablished by a routing and spectrum assignment (RSA) algorithm. Bit rate requirement, routes, distance and modulation format are listed in Table 2. The physical layer parameters values of the elastic optical network are illustrated in Table 3, [4], [21], [22], [26], [36], [37]. Herein, we evaluate only twelve channels, including the channels with higher and lower power transmitted power, to avoid burden information.

B. IPO PROCEDURE UNDER PERFECT CHANNEL CONDITIONS

This step is very important for EON operation under all the operation conditions, such as uncertainty of SNR monitoring,

TABLE 3. Physical layer parameters.

Description	Variable	Value
Bit-error-rate acceptable at pre-FEC [21]	BER*	$4 \cdot 10^{-3}$
Minimum Tx power	$p_{\min}$ (dBm)	-100
Maximum Tx power	$p_{\max}$ (dBm)	20
Channel spacing	Δf (GHz)	50
Planck constant [38]	h (J/Hz)	$6.6261 \cdot 10^{-34}$
Light frequency [38]	v_c (Hz)	$193.55 \cdot 10^{12}$
Group Velocity Dispersion (GVD) [38]	β_2 (s^2/km)	$2.07 \cdot 10^{-23}$
Nonlinear parameter of the fiber [21]	γ (W/km)	1.3
Span length with standard single mode [21]	L (km)	100
Uncertain SNR monitoring, [26]	ϵ_i (dB)	$\sim \mathcal{LN}(\mu, \sigma)$
Standard deviation of ϵ [26]	σ (dB)	[0; 0.16]
Expectation of ϵ [26]	μ (dB)	0
Margin Residual tolerance for lower bound	Λ_1	4E−3
Tolerance adopted for the upper bound of the residual margin	Λ_2	1E−3
Maximum power perturbation [37]	A_{pert} (dB)	1
Begin-of-Life (BoL)	τ_0 (years)	0
End-of-Life (EoL)	τ_{end} (years)	10
Conditional probability of success (CPoS) target	$\mathcal{P}s^*$	0.94
Equipment Ageing Effect		**BoL** **EoL**
Fiber loss coefficient [4]	α_f (dB/km)	0.22 0.23
Connector Loss [4]	c_{loss} (dB)	0.20 0.30
Connectors per span [4]	s_{loss}	2 2
Splice Loss [4]	s_{loss} (dB)	0.30 0.50
Number of splices [4]	s_e (km^{-1})	2 2
EDFA noise figure [4]	N_e (dB)	4.50 5.50
ROADM loss [4]	A^{ROADM} (dB)	20.0 23.0
Transponder Margin [4]	M_t (dB)	1.00 1.50
Design Margin [4]	M_d (dB)	2.00 1.00

effects of ageing and power instability. For this reason, the IPO-performance and IPO-Complexity are treated in the next subsections (V-B.1 to V-B.3), assuming the EON operating under perfect channel conditions, which is given by: perfect estimation of SNR, operation at the BoL and static scenario, following the Table 2 and 3, for operation at any conditions. The round-trip delay are compensated from traditional Smith predictor [31].

Basically, there are four main input parameters, which can be divided into two groups: input parameters that affect directly the performance, given by initial value of the power increasing r_0 and the tangential velocity for the power increasing ω^{WP}; and input parameters that affect directly the CC of the PA algorithms, given by wind parcels K and iterations number N_f. The optimization of both groups is discussed in the subsections V-B.1 and V-B.2, respectively. Others input parameters are described in Table 4. Finally, the IPO under the perspective of complexity-performance tradeoff is elaborated in subsection V-B.3.

1) IPO-PERFORMANCE UNDER PERFECT CHANNEL CONDITIONS

In this context, r_0 and ω^{WP} affect drastically the algorithm's performance. The optimized values are obtained by the IPO-GS framework previously described in section IV-D.1. It assumed $\omega^{\text{WP}} = 1.5708$ as an initial value for the tangential velocity, number of wind parcels $K = 180$ and number of iterations equal to $N_f = 250$, all defined empirically.

Fig. 3 illustrates the r_0 and ω^{WP} optimization across the loops, in such a way that all the optimized parameters reach full convergence. Different ω^{WP} and r_0 values were

TABLE 4. PA-CHSO and -HSO parameters.

Param.	Description	Value
$\omega^{\text{WP}}_{\min}$	Minimum angular velocity	$10^{-4}\cdot\pi$
$\omega^{\text{WP}}_{\max}$	Maximum angular velocity	$2\,\pi$
ω^{WP}	Angular velocity	$[10^{-3}; 2\pi]$
r_0	power increasing [dBm]	$[-100; 20]$
M	Search space dimension or channels number	12
K	Wind parcels number	$M\cdot N_w$
N_f	Number of iterations	$[100; 500]$
N_{lps}	number of loops in the IPO procedure	30
N_r	Number of realizations	100
N_w	Wind parcels factor	$[1; 20]$
$\theta_{k,1}$	Initial angles of the kth wind-parcel	0
θ_k	Angles of the kth wind-parcel	$z_{k,n}$
$\mathbf{p}$	Initial eye (dBm)	0
$z_{k,n}$	Chaotic variable	$[0; 1]$
μ	Control variable of the chaotic logistic map	4
υ	J_1 weighting	1

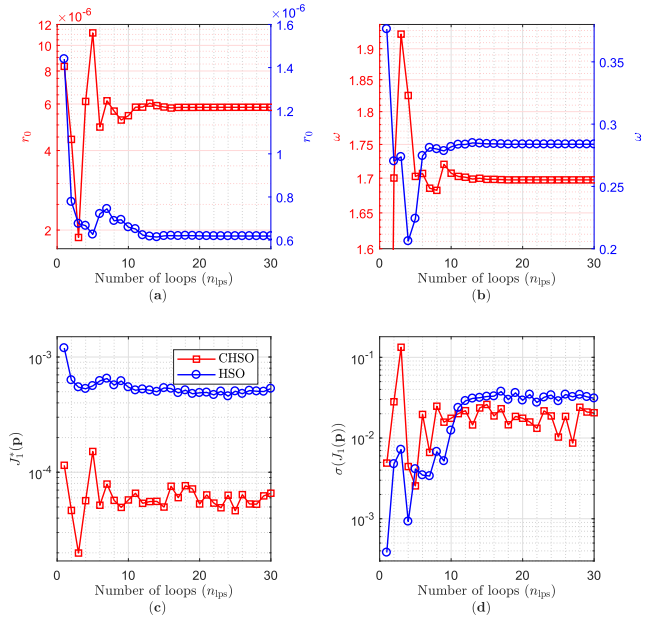

FIGURE 3. Input parameters optimization for the PA-HSO and -CHSO. a) ω^{WP} optimization; b) r_0 optimization; c) the best value of cost function $J_1^*(\mathbf{p})$ in N_r realizations; d) standard deviation for $J_1(\mathbf{p})$.

obtained for both algorithms in Fig. 3.a) and 3.b), demonstrating that the higher parameters values from PA-CHSO perform more accelerated and exploitive (via map chaotic) searches. Consequently, the PA-CHSO found a better solutions, measured by the cost function $J_1(\mathbf{p})$ during N_r realizations and their respective standard deviation, as depicted in Figs. 3.c) and 3.d). More details are listed in Table 5, considering three loops that describe the optimization trend, i.e., $n_{\text{lps}} \in [1;\ 15;\ 30]$; the finals optimized parameters is highlighted by bold face, while the parameters kept fixed at each loop is underlined.

In addition to the proposed optimization by the IPO-GS framework, we perform a numerical analysis IPO-CPoS for the performance input parameters, previously described in

TABLE 5. Performance of the IPO procedure for the PA-CHSO and -HSO.

n_{lps}	Alg.	r_0	ω^{WP}	$J_1^*(\mathbf{p})$	$\sigma(J_1(\mathbf{p})\|\omega^{\text{WP}}, r_0)$
1	PA-CHSO	8.3311E-06	1.5708	1.1493E-04	4.8946E-03
	PA-HSO	1.4398E-06	1.5708	1.1961E-03	3.8201E-04
1	PA-CHSO	8.3311E-06	9.1054E-01	1.1493E-04	4.8946E-03
	PA-HSO	1.4398E-06	3.7636E-01	1.1961E-03	3.8201E-04
-	⋮	⋮	⋮	⋮	⋮
15	PA-CHSO	5.8452E-06	1.6998	4.9901E-05	2.6051E-02
	PA-HSO	6.1944E-07	2.8458E-01	5.3867E-04	3.2671E-02
15	PA-CHSO	5.8452E-06	1.6982	4.9901E-05	2.6051E-02
	PA-HSO	6.1944E-07	2.8418E-01	5.3867E-04	3.2671E-02
-	⋮	⋮	⋮	⋮	⋮
30	PA-CHSO	5.8318E-06	1.6975	6.2371E-05	2.1000E-02
	PA-HSO	6.1873E-07	2.8386E-01	5.0139E-04	3.2378E-02
30	PA-CHSO	**5.8318E-06**	**1.6975**	6.5770E-05	2.0588E-02
	PA-HSO	**6.1873E-07**	**2.8386E-01**	5.3229E-04	3.1103E-02

section IV-D.2, specifically in eq (21). In this numerical analysis, $n \in [1; N_f]$ and $r_0 \in [10^{-8}; 10^{-4}]$, both from Table 5. The ω^{WP} parameter is not evaluated, so it assumes the optimized value from the Table 5.

From eq (21), $\mathcal{P}s_1$ adopts $\Lambda_1 = 4\cdot10^{-3}$ and $\Lambda_2 = 1\cdot10^{-3}$, implying in a $\Psi_{\max} = 10\log 10\,(1.001) = 4.341\cdot10^{-3}$ dB and a $\Psi_{\min} = 10\log 10\,(0.996) = -1.7407\cdot10^{-2}$ dB for the EON system of Table 5. Assuming an average behavior over N_r realizations for the $\mathcal{P}_{s_1}$, the Fig. 4 depicts the IPO-CPoS $\mathcal{P}s_1$ as a function of r_0 and number of iterations from the PA-CHSO and PA-HSO.

As can be observed in Fig. 4, both strategies have attained success, defined as $\mathcal{P}s_1 \geq \mathcal{P}s^*$. In the case of PA-CHSO, a wider range of success regarding PA-HSO has been achieved, defined by $r_0 \in [5\cdot10^{-6};\ 5\cdot10^{-5}]$, and showing that the algorithm presents robustness and lower sensibility during the IPO-CPoS procedure. The best value for the PA-CHSO input parameter is obtained as $r_0^* = 5\cdot10^{-6}$, achieving fast convergence ($n = 50$) and superior performance, *i.e.*, $\mathcal{P}s_1 = 1$. On the other hand, under PA-HSO, the CPoS is found for a narrow range of power increment, $r_0^* \in [6\pm0.5]\cdot10^{-7}$, because adopting similar values, such as $r_0 = 6\cdot10^{-7}$ or $r_0 = 8\cdot10^{-7}$ did not allow PA-HSO achieve $\mathcal{P}s_1 \geq \mathcal{P}s^*$. Hence, PA-HSO presented lower robustness and greater sensibility in adjusting its input parameter in the IPO step. Besides, the PA-HSO found slower convergence and worse performance: $\mathcal{P}s_1(50) = 0$; and $\mathcal{P}s_1(250) = 0.98$, both at r_0^*.

Summarizing, the best r_0 and ω^{WP} parameters found are registered in the last row of Table 5. Varying r_0 with fixed ω^{WP}, $\mathcal{P}s_1$ found a range of r_0 that achieved success for both algorithms. This range defines the ability of updating power, which is directly related to robustness from both algorithms. Hereafter, we adopt for any condition of network's operation: $r_0 \in [5\cdot10^{-6};\ 5\cdot10^{-5}]$ and $\omega^{\text{WP}} = 1.6975$ for the PA-CHSO; and $r_0 \in [6\pm0.5]\cdot10^{-7}$ and $\omega^{\text{WP}} = 2.8386\cdot10^{-1}$ for the PA-HSO.

2) IPO-COMPLEXITY UNDER PERFECT CHANNEL CONDITIONS

K and N_f are the parameters that affect drastically the algorithm's complexity. Then, $\mathcal{P}s_2$ optimizes K given N_f,

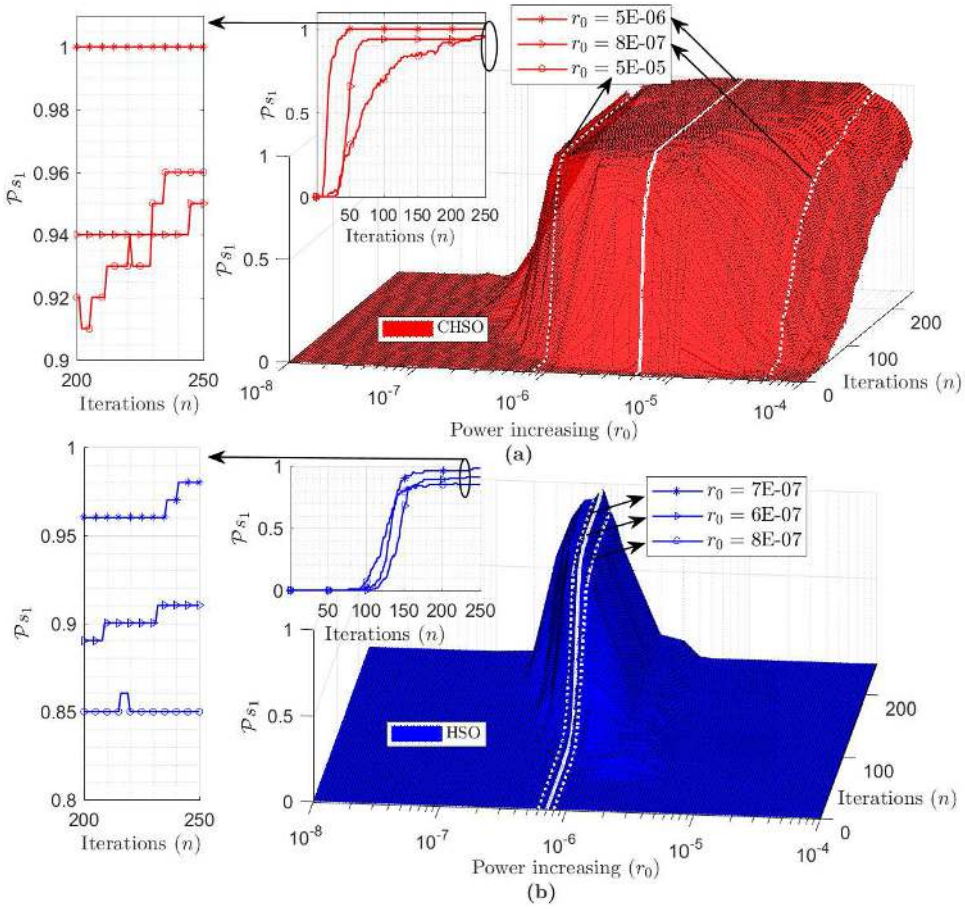

FIGURE 4. IPO-performance: Conditional probability of success ($\mathcal{P}s_1$): a) PA-CHSO; b) PA-HSO.

as described in subsection IV-D.2, specifically in eq. (22). From previous subsection, it was adopted $r_0 = 5.8318 \cdot 10^{-6}$ and $\omega^{\text{WP}} = 1.6975$, for the PA-CHSO; and $r_0 = 6.1873 \cdot 10^{-7}$ and $\omega^{\text{WP}} = 2.8386 \cdot 10^{-1}$, for the PA-HSO. Assuming, an average behavior of N_r realizations, the Fig 5 depicts $\mathcal{P}s_2$ from both algorithms.

As can be observed in Fig 5, a set of infinite number of pairs combinations (K; N_f) found the CPoS, defined as $\mathcal{P}s_2 \geq 0.94$. Thus, to highlight the reliable and feasible region, Fig 5. a) and 5. b) illustrate (green curve) the PF, which is composed by all success points (K^*; N_f^*) assumed as reliable and viable, i.e., eq. (23).

In terms of PF, the PA-CHSO results are better than PA-HSO, showing a wider region for valid pairs (N_f; K), while providing higher regularity in the plane that corresponds to the reliable and feasible region, combined to lower pairs values.

3) PERFORMANCE-COMPLEXITY TRADEOFF

Under channel perfect conditions, the group of input parameters ω^{WP}, r_0, K and N_f are evaluated in terms of performance-complexity tradeoff, in subsection IV-D.2, specifically in eq. (24). The feasible solutions are given by the optimized values of r_0 and ω^{WP}, and PF obtained from the pairs (K, N_f) in Fig 5. As a result, we have found a better performance-complexity tradeoff for the PA-CHSO regarding the PA-HSO, where the best solution for the PA-CHSO is defined as $K = 132$ and $N_f = 180$, i.e., $\mathcal{C}^{\text{PA-CHSO}} = 17.3705$ M flops. While the best solution for the PA-HSO is defined by $K = 228$ and $N_f = 150$, i.e., $\mathcal{C}^{\text{PA-HSO}} = 24.986$ M flops. This IPO framework is summarized in Table 6.

TABLE 6. PA-CHSO and -HSO - Optimized Input Parameters and respective CC ($\mathcal{C}$).

Algorithm	r_0	ω^{WP}	K	N_f	$\mathcal{C}$ [Mflops]
PA-CHSO	$[5.10^{-6};\ 5.10^{-5}]$	1.6975	132	180	17.371
PA-HSO	$[6 \pm 0.5] \cdot 10^{-7}$	0.2839	228	150	24.986

C. PA UNDER PERFECT CHANNEL CONDITIONS

Assuming IPO procedure has been performed previously, the PA per channel across iterations can be obtained, as illustrated in Fig. 6. In the simulations, it has been assumed perfect channel estimation, optical network operating at the BoL and static scenario, with routes, distances and bit rates given

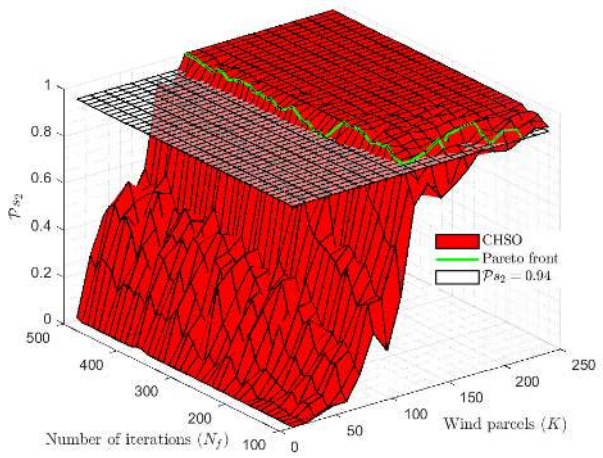

(**a**) CHSO.

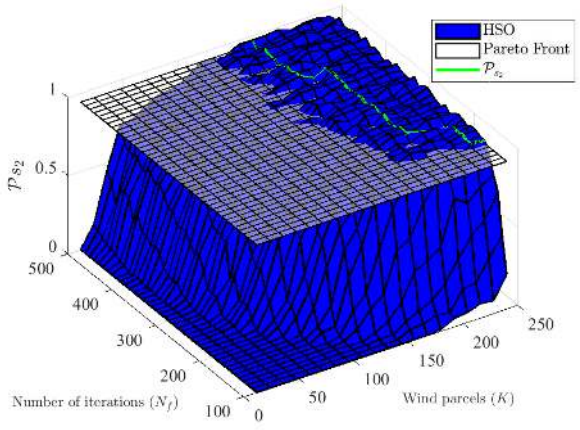

(**b**) HSO

FIGURE 5. **IPO-complexity: conditional probability of success $\mathcal{P}s_2$.**

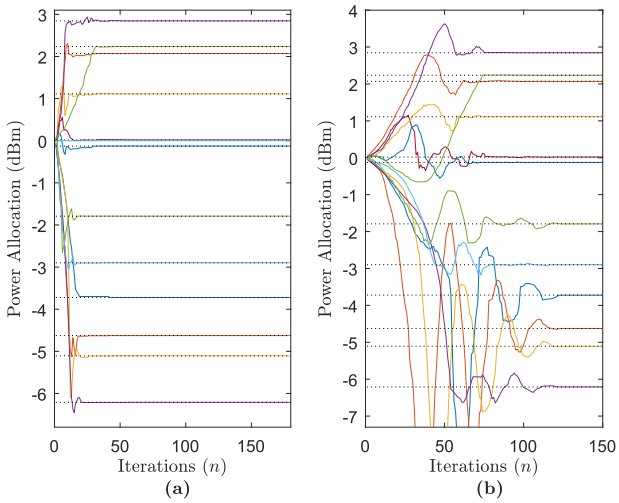

FIGURE 6. **PA per channel *versus* the number of iterations: a) PA-CHSO; b) PA-HSO. Dashed lines in both graphs represent GD solution.**

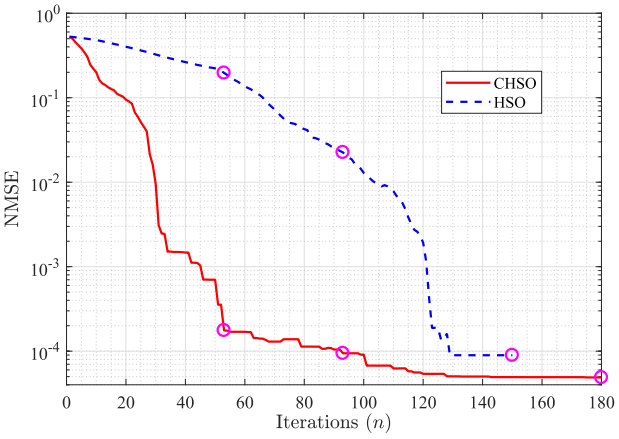

(**a**) Perfect channel conditions

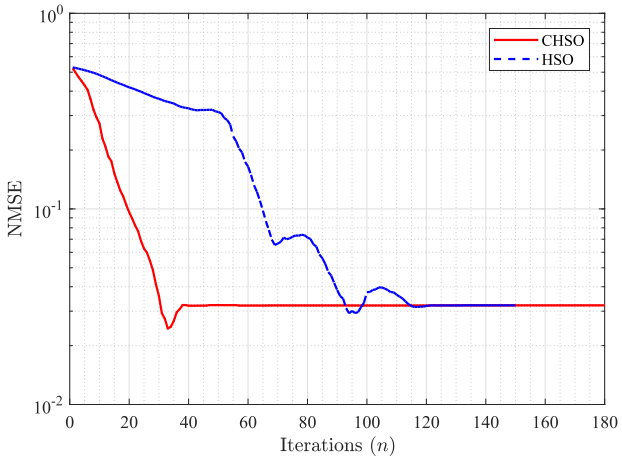

(**b**) Imperfect channel conditions

FIGURE 7. **Normalized mean square error (nmse) against the number of iterations for PA-CHSO and -HSO algorithm operating under perfect and imperfect channel conditions.**

in Table 2, as well as physical parameters values following Table 3. The general parameters of the PA algorithms are adopted from the Table 4, while performance and CC parameters are adopted from the Table 6, being $r_0 = 5.8318 \cdot 10^{-6}$ (PA-CHSO) and $r_0 = 6.1873 \cdot 10^{-7}$ (PA-HSO). Indeed, the PA per channel reaches full convergence for both PA algorithms. The horizontal dashed lines represent the PA per channel obtained via GD procedure, which is an analytical method that has been used to validate convergence of the PA-CHSO and PA-HSO.

Regarding the results in Fig. 6, the following metrics have been calculated to the PA-CHSO and -HSO: *a*) the mean integral absolute value of the residual margin for the M-channels during time-window resulted equal to 19.1287 dB and 23.1334 dB, respectively; the maximum PP all the channels ($\max(\overline{\mathbf{p}})$) at the last iteration of $3.3811{\cdot}10^{-4}$ dB and $1.4014{\cdot}10^{-3}$ dB, respectively; *b*) mean settling iteration of all the users ($\overline{i_s}$), assuming tolerance around 10^{-4} for the M channels (i.e., $\mathbf{p}^* - \mathbf{p} \leq 1 \cdot 10^{-7}$), results in ≈ 79 and ≈ 129 iterations, respectively. In this sense, the superiority from the PA-CHSO is evident. Besides, Fig. 6 presents overshooting and undershooting during the PA, which is much more noticiable in the PA-HSO convergence. This behaviour is called sub-damped, where the transient responses are oscillatory and the closed-loop poles are complex conjugates.

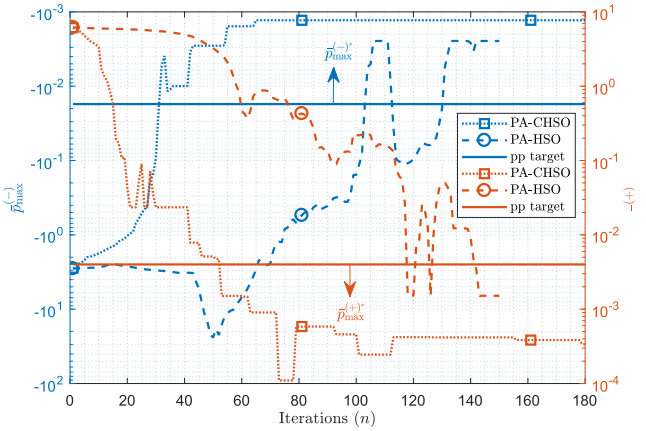

FIGURE 8. Maximum and minimum penalty power, i.e., $\bar{p}^{(+)}_{\max}$ and $\bar{p}^{(-)}_{\max}$, and theirs target values, i.e., $\bar{p}^{(+)*}_{\max}$ and $\bar{p}^{(-)*}_{\max}$, against the number of iterations for PA-CHSO and -HSO.

Fig. 7.a) depicts the quality of the solution by the NMSE analysis from Fig. 6. In this figure, three main behaviors are highlighted through the circles c_1, c_2 and c_3. The point $c_1(n = 53)$ represents the ability of the PA-CHSO to find a better candidate solution in few iterations, *i.e.*, it found a NMSE $= 1.76 \cdot 10^{-4}$, while the PA-HSO was able to attain NMSE$= 0.1965$. The intermediate point c_2 ($n = 93$) represents the PA-CHSO around a good candidate solution, in consequence of its more exploitative nature, it is a region which the PA-CHSO can be slower than PA-HSO. In this region, the NMSE reduction are of order of $2.0451 \cdot 10^{-6}$ and $9.4385 \cdot 10^{-5}$, for PA-CHSO; and $4.3480 \cdot 10^{-3}$ and $= 2.2552 \cdot 10^{-2}$, for PA-HSO. c_3 represents the PA-CHSO ability to achieve a better solution at the last iteration: the PA-CHSO found a NMSE$= 4.87768 \cdot 10^{-5}$; and PA-HSO found a NMSE$= 8.9501 \cdot 10^{-5}$ for the PA-HSO. Besides, in range of $n = 1$ to 53 is evident the instability by PA-HSO, due to its lower exploitative capacity for the power launch (or initial power of the eye) of 0 dbm. Therefore, the best PA capacity from PA-CHSO is clear.

Fig 8 depicts the quality of the solution by the PP analysis from Fig. 6, illustrating $\bar{p}^{(-)}_{\max}$ and $\bar{p}^{(+)}_{\max}$ of the M channels across the n. Here, it is adopted that $\Psi_{\min}$ and $\Psi_{\max}$ values define the minimum target values for $\bar{p}^{(-)}_{\max}$ and $\bar{p}^{(+)}_{\max}$, denoted as $\bar{p}^{(-)*}_{\max}$ and $\bar{p}^{(+)*}_{\max}$, respectively. The $\bar{p}^{(-)}_{\max}$ and $\bar{p}^{(+)}_{\max}$ results show that the PA-CHSO outperforms the PA-HSO, i.e., it guarantees $\Psi_{\min}$ at $n \geq 31$ and $\Psi_{\max}$ at $n \geq 53$, while the PA-HSO guarantees $\Psi_{\min}$ at $n \geq 131$ and $\Psi_{\max}$ at $n \geq 141$. The final values found for the PA-CHSO are $\bar{p}^{(+)}_{\max}[180] = 3.3811 \cdot 10^{-4}$ and $\bar{p}^{(-)}_{\max}[180] = -1.2971 \cdot 10^{-3}$, while for the PA-HSO are $\bar{p}^{(+)}_{\max}[150] = 1.5164 \cdot 10^{-3}$ and $\bar{p}^{(-)}_{\max}[150] = -2.4642 \cdot 10^{-3}$, respectively. Therefore, it is evident the energy saving from the PA-CHSO.

D. PA UNDER IMPERFECT CHANNEL CONDITIONS

In order to evaluate the PA-CHSO and -HSO effectiveness in terms of optimal PA, three analysis for channel conditions were carried out: a) non-perfect monitoring of the OPMs, in section V-D.1; b) channel ageing effects, in section V-D.2; c) power instability, in section V-D.3. The general parameters values adopted for both algorithms are described Table 4, while input parameters are depicted in Table 6, with the choice of $r_0 = 5.8318 \cdot 10^{-6}$ (PA-CHSO) and $r_0 = 6.1873 \cdot 10^{-7}$ (PA-HSO).

1) NON-PERFECT MONITORING OF THE OPMs

there is an inaccuracy in the monitoring of the OPMs. Here, it is considered as a random variable $\epsilon_i \sim \mathcal{LN}(\mu, \sigma)$, where $\mu = 0$ dB and $\sigma = 0.16$ dB. These monitoring uncertainties corresponds to a maximum error $\epsilon_{i_{\max}} = 0.6$ dB with high probability (> 0.9995), commonly adopted in the optical networks considering inaccuracies from the OPMs [38]–[40]. This error is added into ith SNR during the PA procedure. Moreover, the adopted scenario assumes an operation at the BoL without power instability.

Fig. 7.b) depicts the velocity and the tendency of convergence, as well as the quality of the solutions. As can be observed, there is a decrease in the NMSE with the increase in the number of iterations. It is noticed that for early iterations the PA-CHSO achieves better convergence performance when compared to PA-HSO. In terms of convergence velocity, the PA-CHSO (at $n = 42$) is able to attain a NMSE $= 3.2 \cdot 10^{-2}$ approximately three times faster than PA-HSO ($n = 123$). On the other hand, similar NMSE values are found in the later iterations, *i.e*, $n \geq 125$ iteration, where both algorithms achieve an asymptotic NMSE $\approx 3.21 \cdot 10^{-2}$. Those results are affected by the OPMs inaccuracies. Indeed, comparing both PA algorithms performance operating under perfect monitoring condition, Fig. 7.a), the same asymptotic NMSE value has not been observed in both schemes. In this ideal scenario, the maximum PP resulted in $p^{\text{pa-chso}}_{i_{\max}} = 0.26042$ dB and $p^{\text{pa-hso}}_{i_{\max}} = 0.26037$ dB.

2) CHANNEL AGEING EFFECTS

Under equipment ageing effects, Fig. 9 proposes analyze the PP trend against a multi-period incremental assuming $\tau = [0, 2, 4, \cdots, 10]$ years, representing the effect of ageing from BoL to EoL network. It illustrates the expected value of the PP from M-channels ($\mathbb{E}[\bar{\mathbf{p}}]$) across the time, as well as their respective standard deviation ($\sigma_{\bar{\mathbf{p}}}$), $\bar{p}^{(+)}_{\max}$ and $\bar{p}^{(-)}_{\max}$. The ageing from the parameters is assumed as a linear function of time τ.

Elaborate further, it is possible to see in Fig. 9, that PA-CHSO performs better when compared to the PA-HSO. $\mathbb{E}[\bar{\mathbf{p}}]$ and $\sigma_{\bar{\mathbf{p}}}$ are measured with the objective of evaluating the lower and upper bound of the PP of M-channels during EON lifetime. Here, it is assumed that $\Psi_{\min}$ and $\Psi_{\max}$ define the minimum values of the PP target, i.e., $\bar{p}^{(-)}_{\max} = -1.7407 \cdot 10^{-2}$ db and $\bar{p}^{(+)}_{\max} = 4.3427 \cdot 10^{-4}$ dB, respectively. Details about $\bar{p}^{(-)}_{\max}$ and $\bar{p}^{(-)}_{\max}$ are in section IV-E.1. In case of the maximum PP, PA-CHSO is better than PA-HSO, achieving a maximum value of $\mathbb{E}[\bar{\mathbf{p}}] \approx 4.3432 \cdot 10^{-4}$ dB at $\tau = 10$

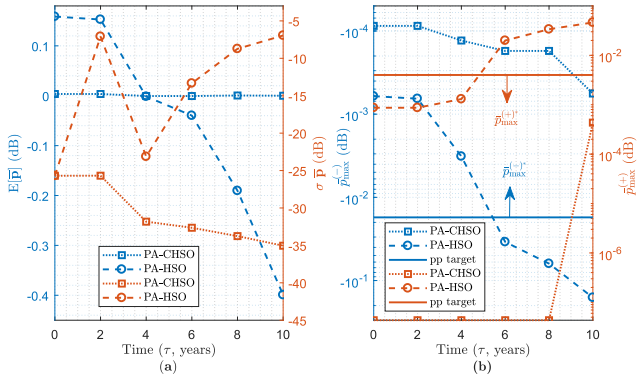

FIGURE 9. **(a) Expected value of power PP for *M*-channels across time at years ($\mathbb{E}[\overline{p}]$) and their respective standard deviation ($\sigma_{\overline{p}}$), (b) $\bar{p}^{(+)}_{\max}$ and $\bar{p}^{(-)}_{\max}$, $\bar{p}^{(+)*}_{\max}$ and $\bar{p}^{(-)*}_{\max}$ values, for the PA-CHSO and PA-HSO.**

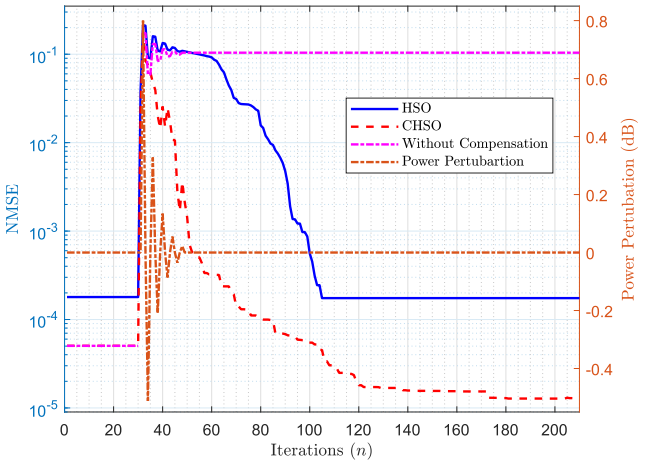

FIGURE 10. NMSE **for a dynamic scenario characterized by a power perturbation (**pert**) occuring in between 30 < *n* ≤ 49 iterations. Two channels are dropped, $\mathcal{R}_{10}$ and $\mathcal{R}_{11}$, and three situation are taken: without compensation and compensation via PA-CHSO and -HSO.**

against $\mathbb{E}[\overline{\mathbf{p}}] \approx 4.6223 \cdot 10^{-2}$ dB at $\tau = 10$. In terms of minimum PP, the PA-CHSO found BER* all the time, a consequence of $\mathbb{E}[\overline{\mathbf{p}}] \approx -5.6462 \cdot 10^{-4}$ dB $\leq \Psi_{\min}$ at $\tau = 10$, while the PA-HSO does not found BER*, a consequence of $\mathbb{E}[\overline{\mathbf{p}}] \approx -1.6013 \cdot 10^{-1}$ dB $\geq \Psi_{\min}$ at $\tau = 10$. Therefore, the PA-CHSO and -HSO resulted at a margin increasing of $5.6462 \cdot 10^{-4}$ dB and $1.6013 \cdot 10^{-1}$ dB, respectively, and presented a better saving energy. Besides, the $\sigma_{\overline{\mathbf{p}}}$ values found demonstrated that PA-CHSO is more stable than PA-HSO in terms of minimum energy expenditure to achieve the BER*. In this context, PA-CHSO is effective to mitigate the channel ageing effects.

3) POWER INSTABILITY

Assuming now a dynamic scenario characterized by power instability or perturbation, which can represent dropping or adding channels to the EON. After node add-drop channels an undesired effect reaches the surviving channels, herein modeled as a sine function in eq. (13), where $A_{\text{pert}} = 0.8$ dB and $f = 0.5$ Hz represents overshoot and undershoot maximum adopted in the project of EDFA compensation of ± 1 dB. Theses values assured the drops of the two routes, simultaneously [36].

In simulations of Fig. 10, a dynamic scenario has been modeled assuming a network optimized to operate with 12 users, such as in Table 2 and Fig. 2. Thus, a fast variation is introduced at the node 8, where $\mathcal{R}_{10}$ and $\mathcal{R}_{11}$ are dropped at the iteration 30. This dropping results in four surviving channels ($\mathcal{R}_4$, $\mathcal{R}_8$, $\mathcal{R}_9$ and $\mathcal{R}_{12}$) forward. These channels are affected by power fluctuations from node 8 to $\mathcal{D}$. The interval of perturbation occurs at $30 < n \leq 49$.

Elaborating furhter, Fig. 10 illustrates the effect of the power perturbation under three situations: with and without compensation from PA-CHSO and -HSO. In case of no compensation, the launch power is assumed as optimized from the PA-CHSO, and power adjustment is not carried out after the drop of the two channels. In other words, the channels $\mathcal{R}_4$, $\mathcal{R}_8$, $\mathcal{R}_9$ and $\mathcal{R}_{12}$ are penalized and theirs transmission power are not re-optimized, resulting in a NMSE[210] $= 1.0406 \cdot 10^{-1}$. However, performance improvment can be attained deploying compensation in PA-HSO and PA-CHSO, resulting in a NMSE[210] $= 1.7455 \cdot 10^{-4}$ and $1.2874 \cdot 10^{-5}$, respectively. It is evident the PA-CHSO ability to escape from local minimum around $n = 100$, as well as the behavior of both algorithms in the sense of following the power perturbation and in achieving the optimal power in latter iterations.

A comparison between the initial and final NMSE value showed that for the PA-HSO, similar values are found, *i.e.*, $\text{NMSE}_1 = 1.7946 \cdot 10^{-4}$ and NMSE[1] $= 1.7455 \cdot 10^{-4}$; and for the PA-CHSO, a better final value is found, *i.e.*, a gap of $\Delta\text{NMSE} = 3.76 \cdot 10^{-5}$. Therefore, the PA assuming fluctuation from drop channels is validated and a better performance is found by the PA-CHSO.

E. COMPLEXITY

The CC is evaluated in terms of mathematical operations and number of channels. In asymptotic terms, the PA-HSO and PA-CHSO have complexity of order of $\mathcal{O}(M^2)$. On the other hand, the complexity of GD algorithm is of order of $\mathcal{O}(M^3)$, as described in section IV-E.2. Aiming at attaining more accuracy in the complexity analyses, we have considered the mathematical operations from eqs. (27), (26) and (28). Three different system loadings have been adopted: **A** has 12 channels (2,2 Tbps), as described in Table 2 and Fig. 2; **B** has 120 channels (22 Tbps); and **C** has 240 channels (44 Tbps). **B** and **C** have the same topology of **A**, however theirs routes result of 10 and 20 times of **A** ($\mathcal{R}_1, \cdots, \mathcal{R}_{12}$), respectively. Those scenarios assume perfect channel conditions: operation at the BoL, static operation, and perfect monitoring of channel.

Fig. 11 depicts the averaged CC for the three algorithms operating under **A**, **B** and **C** scenarios. It also assumes optimized parameters from the Table 6. Those parameters result the worst-case for the CC, i.e., K and N_f can be reduced

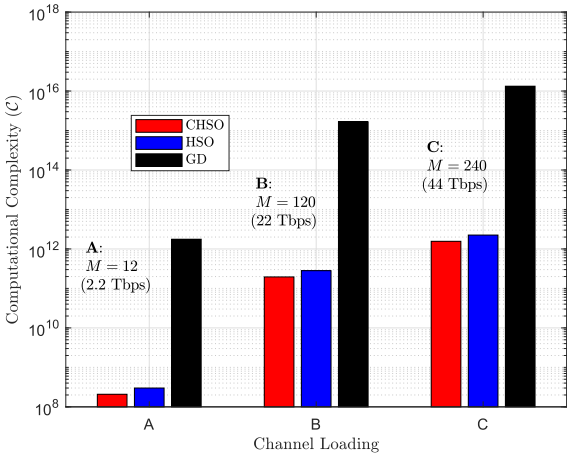

FIGURE 11. Complexity computational for three different channel scenarios: PA-CHSO, -HSO and -GD.

due to the increasing of M-channels and r_0, while ω^{WP} can be reduced due to the increasing of non-linear effect. The PA-CHSO has resulted in lower complexity than two methods. In addition, the CC can be reduced by considering re-optimization of input parameters for any network operating conditions.

VI. CONCLUSION

The PA-CHSO method proved to be a promising technique to resource allocation in elastic optical networks, especially by Nyquist wavelength division multiplexing (WDM) super-channels, combining competitive convergence speed, control capacity, non-linear effects mitigation, higher probability of success in lower iterations and lower penalties. The PA-CHSO has demonstrated a higher ability to escape of local minimum caused by non-linear effects in scenarios where higher bit rates are required. The optimized parameters presented robustness considering conditional probability of success. Moreover, it resulted in a CC in the order of $\mathcal{O}(M^2)$, much lower than the gradient descent method (of order of $\mathcal{O}(M^3)$), and marginally lower compared to the conventional PA-HSO.

The conventional PA-HSO has presented inferior performance regarding the PA-CHSO. In terms of the optimization of parameters, a narrow conditional probability of success was found, resulting in a low ability for absorption of ageing effects and vast-variations, a consequence of higher sensibility to the parameters variation. Moreover, it was found worse penalties and lower convergence speed in case of dynamic scenarios.

The PA-CHSO performs PA in EONs with better performance-complexity tradeoff regarding both the PA-HSO and the PA-GD, considering non-perfect monitoring of OPMs, channel ageing effects and dynamic scenario, that are the main realistic conditions from EONs operations. Such advantages result in a better margin reduction, energy efficiency improvement, and cost limitations. In summary, inserting chaotic map procedure into the PA-HSO (or -CHSO) brought better performance-complexity balancing tradeoff.

ACKNOWLEDGMENT

This work has been partially supported by the National Council for Scientific and Technological Development (CNPq) of Brazil under Grants 304066/2015-0; in part by the Coordenação de Aperfeiçoamento de Pessoal de Nível Superior - Brazil (CAPES) - Finance Code 001'', and by the Londrina State University (UEL), the Paraná State Government, and in part by CAPES and Federal University of Technology - Parana State (UTFPR). All the agencies are gratefully acknowledged. Dr. Fábio Renan Durand, died on August 30th, 2019, is gratefully acknowledged; he was an advisor of the authors; and published several works in the IEEE in the last years.

REFERENCES

[1] A. Klekamp and U. Gebhard, ''Performance of elastic and mixed-line-rate scenarios for a real ip over dwdm network with more than 1000 nodes,'' *J. Opt. Commun. Netw.*, vol. 5, no. 10, pp. A28–A36, 2013.

[2] P. Soumplis, K. Christodoulopoulos, M. Quagliotti, A. Pagano, and E. Varvarigos, ''Multi-period planning with actual physical and traffic conditions,'' *IEEE/OSA J. Opt. Commun. Netw.*, vol. 10, no. 1, pp. A144–A153, Jan. 2018.

[3] M. Kanj, E. Le Rouzic, J. Meuric, and B. Cousin, ''Optical power control in translucent flexible optical networks with GMPLS control plane,'' *IEEE/OSA J. Opt. Commun. Netw.*, vol. 10, no. 9, pp. 760–772, Sep. 2018.

[4] P. Soumplis, K. Christodoulopoulos, M. Quagliotti, A. Pagano, and E. Varvarigos, ''Network planning with actual margins,'' *J. Lightw. Technol.*, vol. 35, no. 23, pp. 5105–5120, Dec. 1, 2017.

[5] B. Birand, H. Wang, K. Bergman, D. Kilper, T. Nandagopal, and G. Zussman, ''Real-time power control for dynamic optical networks—Algorithms and experimentation,'' *IEEE J. Sel. Areas Commun.*, vol. 32, no. 8, pp. 1615–1628, Aug. 2014.

[6] L. R. R. dos Santos, F. R. Durand, and T. Abrao, ''Adaptive power control algorithm for dynamical transmitted power optimization in mixed-line-rate optical networks,'' *IEEE Commun. Lett.*, vol. 22, no. 10, pp. 2032–2035, Oct. 2018.

[7] E. Seve, J. Pesic, C. Delezoide, S. Bigo, and Y. Pointurier, ''Learning process for reducing uncertainties on network parameters and design margins,'' *J. Opt. Commun. Netw.*, vol. 10, no. 2, pp. A298–A306, Feb. 2018.

[8] M. Bouda, S. Oda, O. Vassilieva, M. Miyabe, S. Yoshida, T. Katagiri, Y. Aoki, T. Hoshida, and T. Ikeuchi, ''Accurate prediction of quality of transmission based on a dynamically configurable optical impairment model,'' *J. Opt. Commun. Netw.*, vol. 10, no. 1, pp. A102–A109, Jan. 2018.

[9] L. D. N. Calleja, S. Spadaro, J. Perelló, and G. Junyent, ''Cognitive science applied to reduce network operation margins,'' *Photonic Netw. Commun.*, vol. 34, no. 3, pp. 432–444, Dec. 2017.

[10] Y. Pan and L. Pavel, ''OSNR game optimization with link capacity constraints in general topology WDM networks,'' *Opt. Switching Netw.*, vol. 11, pp. 1–15, Jan. 2014.

[11] C. Rottondi, L. Barletta, A. Giusti, and M. Tornatore, ''Machine-learning method for quality of transmission prediction of unestablished lightpaths,'' *IEEE/OSA J. Opt. Commun. Netw.*, vol. 10, no. 2, pp. A286–A297, Feb. 2018.

[12] C. A. Pendeza Martinez, F. R. Durand, and T. Abrao, ''Energy-efficient QoS-based OCDMA networks aided by nonlinear programming methods,'' *AEU-Int. J. Electron. Commun.*, vol. 98, pp. 144–155, Jan. 2019, doi: 10.1016/j.aeue.2018.11.007.

[13] L. Kumar, V. Sharma, and A. Singh, ''Feasibility and modelling for convergence of optical-wireless network–a review,'' *AEU-Int. J. Electron. Commun.*, vol. 80, pp. 144–156, Oct. 2017, doi: 10.1016/j.aeue.2017.06.027.

[14] I. Roberts, J. M. Kahn, and D. Boertjes, ''Convex channel power optimization in nonlinear WDM systems using Gaussian noise model,'' *J. Lightw. Technol.*, vol. 34, no. 13, pp. 3212–3222, Jul. 1, 2016.

[15] S. Boyd and L. Vandenberghe, *Convex Optimization*. Cambridge, U.K.: Cambridge Univ. Press, 2004.
[16] L. dos Santos Coelho and V. C. Mariani, "Use of chaotic sequences in a biologically inspired algorithm for engineering design optimization," *Expert Syst. Appl.*, vol. 34, no. 3, pp. 1905–1913, 2008.
[17] B. Alatas, E. Akin, and A. B. Ozer, "Chaos embedded particle swarm optimization algorithms," *Chaos, Solitons Fractals*, vol. 40, no. 4, pp. 1715–1734, May 2009.
[18] I. Rbouh and A. A. E. Imrani, "Hurricane-based optimization algorithm," *AASRI Procedia*, vol. 6, pp. 26–33, Jun. 2014.
[19] R. M. Rizk-Allah, R. A. El-Sehiemy, and G.-G. Wang, "A novel parallel hurricane optimization algorithm for secure emission/economic load dispatch solution," *Appl. Soft Comput.*, vol. 63, pp. 206–222, Feb. 2018.
[20] A. H. Gandomi, X.-S. Yang, S. Talatahari, and A. H. Alavi, "Firefly algorithm with chaos," *Commun. Nonlinear Sci. Numer. Simul.*, vol. 18, no. 1, pp. 89–98, Jan. 2013.
[21] L. Yan, E. Agrell, H. Wymeersch, and M. Brandt-Pearce, "Resource allocation for flexible-grid optical networks with nonlinear channel model [invited]," *J. Opt. Commun. Netw.*, vol. 7, no. 11, pp. B101–B108, Nov. 2015.
[22] P. Poggiolini, G. Bosco, A. Carena, V. Curri, Y. Jiang, and F. Forghieri, "The GN-model of fiber non-linear propagation and its applications," *J. Lightw. Technol.*, vol. 32, no. 4, pp. 694–721, Feb. 15, 2014.
[23] K. Cho and D. Yoon, "On the general BER expression of one- and two-dimensional amplitude modulations," *IEEE Trans. Commun.*, vol. 50, no. 7, pp. 1074–1080, Jul. 2002.
[24] A. Carena, V. Curri, G. Bosco, P. Poggiolini, and F. Forghieri, "Modeling of the impact of nonlinear propagation effects in uncompensated optical coherent transmission links," *J. Lightw. Technol.*, vol. 30, no. 10, pp. 1524–1539, May 15, 2012.
[25] Y. Pointurier, "Design of low-margin optical networks," *IEEE/OSA J. Opt. Commun. Netw.*, vol. 9, no. 1, pp. A9–A17, Jan. 2017.
[26] I. Sartzetakis, K. K. Christodoulopoulos, and E. M. Varvarigos, "On reducing optical monitoring uncertainties and localizing soft failures," in *Proc. IEEE Int. Conf. Commun. (ICC)*, May 2017, pp. 1–6.
[27] A. Nag, M. Tornatore, and B. Mukherjee, "On the effect of channel spacing, launch power, and regenerator placement on the design of mixed-line-rate optical networks," *Opt. Switching Netw.*, vol. 10, no. 4, pp. 301–311, Nov. 2013.
[28] J. Pesic, T. Zami, P. Ramantanis, and S. Bigo, "Faster return of investment in WDM networks when elastic transponders dynamically fit ageing of link margins," in *Proc. Opt. Fiber Commun. Conf.*, Mar. 2016, pp. 1–3.
[29] S. Iyer and S. P. Singh, "Investigation of launch power and regenerator placement effect on the design of mixed-line-rate (MLR) optical WDM networks," *Photon. Netw. Commun.*, pp. 1–17, Jun. 2017, doi: 10.1007/s11107-017-0714-z.
[30] L. D. H. Sampaio, T. Abrão, B. A. Angélico, M. F. Lima, M. L. Proença, and P. J. E. Jeszensky, "Hybrid heuristic-waterfilling game theory approach in MC-CDMA resource allocation," *Appl. Soft Comput.*, vol. 12, no. 7, pp. 1902–1912, Jul. 2012.
[31] T. A. B. Alves, F. R. Durand, B. A. Angélico, and T. Abrão, "Power allocation scheme for OCDMA NG-PON with proportional–integral–derivative algorithms," *J. Opt. Commun. Netw.*, vol. 8, no. 9, pp. 645–655, Sep. 2016.
[32] J. C. M. Filho, R. N. de Souza, and T. Abrão, "Ant colony input parameters optimization for multiuser detection in DS/CDMA systems," *Expert Syst. Appl.*, vol. 39, no. 17, pp. 12876–12884, Dec. 2012.
[33] M. Tang, C. Long, and X. Guan, "Nonconvex optimization for power control in wireless CDMA networks," *Wireless Pers. Commun.*, vol. 58, no. 4, pp. 851–865, Jun. 2011.
[34] F. R. Durand and T. Abrão, "Energy-efficient power allocation for WDM/OCDM networks with particle swarm optimization," *J. Opt. Commun. Netw.*, vol. 5, no. 5, pp. 512–523, 2013.
[35] W. Press, B. Flannery, S. Teukolsky, and W. Vetterling, *Numerical Recipes: The Art of Scientific Computing*. Cambridge, U.K.: Cambridge Univ. Press, 1986.
[36] V. A. C. Vale and R. C. Almeida, "Power, routing, modulation level and spectrum assignment in all-optical and elastic networks," *Opt. Switching Netw.*, vol. 32, pp. 14–24, Apr. 2019.
[37] J. Tsai, Z. Wang, Y. Pan, D. C. Kilper, and L. Pavel, "Stability analysis in a ROADM-based multi-channel quasi-ring optical network," *Opt. Fiber Technol.*, vol. 21, pp. 40–50, Jan. 2015.
[38] Z. Dong, F. N. Khan, Q. Sui, K. Zhong, C. Lu, and A. P. T. Lau, "Optical performance monitoring: A review of current and future technologies," *J. Lightw. Technol.*, vol. 34, no. 2, pp. 525–543, Jan. 15, 2016.
[39] A. E. Willner, Z. Pan, and C. Yu, "Optical performance monitoring," in *Optical Fiber Telecommunications V B*. Amsterdam, The Netherlands: Elsevier, 2008, pp. 233–292.
[40] W. Shieh, R. S. Tucker, W. Chen, X. Yi, and G. Pendock, "Optical performance monitoring in coherent optical OFDM systems," *Opt. Express*, vol. 15, no. 2, pp. 350–356, Jan. 2007.

LAYHON R. RODRIGUES DOS SANTOS received the B.S. degree in electrical engineering from the North Paraná University, in 2016, and the M.S. degree in electrical engineering from the Technologic Federal University of Paraná (UTFPR), Cornélio Procópio, Brazil, in 2018. He is currently pursuing the Ph.D. degree in electrical engineering with Londrina State University (UEL)/UTFPR-CP Association, Brazil. His research interest includes the optimization aspects of photonic technology involving resource allocation and energy efficiency. Besides, it has been dealing with the concept and implementation of new heuristic methods based on artificial intelligence.

TAUFIK ABRÃO (Senior Member, IEEE) received the B.S., M.Sc., and Ph.D. degrees in electrical engineering from the Polytechnic School of the University of São Paulo, São Paulo, Brazil, in 1992, 1996, and 2001, respectively. Since March 1997, he has been with the Communications Group, Department of Electrical Engineering, Londrina State University, Londrina, Brazil, where he is currently an Associate Professor of telecommunications and the Head of the Telecomm and Signal Processing Laboratory. He is also a Productivity Researcher with the CNPq Brazilian Agency (Pq-1D). From July to October 2018, he was with the Connectivity Section, Aalborg University as a Guest Researcher. In 2012, he was an Academic Visitor with the Southampton Wireless Research Group, University of Southampton, Southampton, U.K. From 2007 to 2008, he was a Postdoctoral Researcher with the Department of Signal Theory and Communications, Polytechnic University of Catalonia (TSC/UPC), Barcelona, Spain. He has participated in several projects funded by government agencies and industrial companies. His current research interests include communications and signal processing, especially massive MIMO, ultrareliable low latency communications, detection and estimation, multicarrier systems, cooperative communication and relaying, resource allocation, as well as heuristic and convex optimization aspects of 5G wireless systems. He has supervised 27 M.Sc. and 4 Ph.D. students, as well as 3 postdocs, coauthored 12 book chapters on mobile radio communications and +280 research articles published in international journals and conferences. Prof. Abrão is a member of SBrT. He is involved in Editorial Board activities of several journals in the telecommunications area and has served as a TPC Member in several symposiums and conferences. He has been serving as an Associate Editor for IEEE Access, since 2016, the *IET Journal of Engineering*, since 2014, the *IET Signal Processing*, since December 2018, and the *JCIS-SBrT Journal*, since 2018. Previously, he served as a AE of the IEEE Communication Surveys and Tutorials, from 2013 to 2017. Moreover, he has been served as an Executive Editor of the *ETT-Wiley Journal*, since 2016.